Aging and Disease
www.aginganddisease.org
Early access date: May 12, 2026
http://dx.doi.org/10.14336/AD.2026.0142

Original Article

circHIPK3 Sustains Ribosome Biogenesis and Protects Against Cardiac Aging by Stabilizing Ncl mRNA and Supporting its LLPS

Huiling Zhang[1#], Tonggan Lu[1#], Xinlan Lv[1], Yu Zhang[1], Ao Li[1], Zirui Zhao[1], Han Zhou[1], Bin Liu[2], Yan Xu[3*], Yangxin Li[1*]

[1]Department of Cardiovascular Surgery of the First Affiliated Hospital & Institute for Cardiovascular Science, Collaborative Innovation Center of Hematology, State Key Laboratory of Radiation Medicine and Protection, Suzhou Medical College, Soochow University, Suzhou, Jiangsu 215123, China. [2]Department of Cardiology, the Second Hospital of Jilin University, Changchun, Jilin 130041, China. [3]Department of General Medicine, the Second Xiangya Hospital, Central South University, Changsha, Hunan 410011, China

[Received January 30, 2026; Revised May 3, 2026; Accepted May 4, 2026]

ABSTRACT: To investigate the molecular mechanism of cardiac aging and identify novel regulatory targets, we focused on circular RNA HIPK3 (circHIPK3) and its role in regulating Nucleolin (Ncl)-mediated biological processes. circHIPK3 expression was progressively downregulated with age in mouse hearts. We generated cardiomyocyte-specific circHIPK3 knockout (CKO) mice, and found that these mice exhibited cardiac aging phenotypes, cardiac dysfunction, hypertrophy, and fibrosis. Mechanistically, circHIPK3 is directly bound to the 5' UTR of Ncl mRNA to enhance its stability, thereby preserving Ncl protein levels and supporting Ncl-mediated liquid-liquid phase separation (LLPS), a critical process for efficient ribosome biogenesis. circHIPK3 deficiency is accompanied by altered Ncl LLPS dynamics, reduced ribosomal RNA synthesis and ribosomal protein expression, and impaired *de novo* ribosome production. Conversely, circHIPK3 overexpression restored Ncl expression, rescued LLPS and ribosome biogenesis defects, and alleviated aging-related cardiac phenotypes *in vitro* and *in vivo*. In conclusion, we identify a novel "circHIPK3-Ncl-ribosome biogenesis" axis that protects against cardiac aging through post-transcriptional and biophysical regulation. circHIPK3 represents a potential biomarker and warrants further investigation as a therapeutic candidate for age-related cardiovascular dysfunction, providing new insights into the intersection of non-coding RNA function, ribosome biogenesis and organ aging.

Keywords: Nucleolin, Ribosome biogenesis, Aging, LLPS

INTRODUCTION

Cardiovascular diseases (CVDs) represent the most significant challenge to global health, accounting for approximately 19.2 million deaths in 2023 and establishing themselves as the leading cause of mortality worldwide [1]. The risk of developing CVDs is strongly and positively associated with advancing age. Aging is not merely a chronological process, but a complex biological phenomenon characterized by progressive functional decline at molecular, cellular, and tissue levels [2]. In the heart, this process manifests as cardiac aging, which is defined by pathological changes including ventricular hypertrophy, reduced contractility, diastolic dysfunction, and excessive myocardial fibrosis. Collectively, these alterations compromise the heart's adaptive capacity to stress [3, 4] and form the critical pathological basis for age-related cardiovascular conditions such as heart failure

***Correspondence should be addressed to:** Dr. Yangxin Li, State Key Laboratory of Radiation Medicine and Protection, Suzhou Medical College, Soochow University, Suzhou, Jiangsu, China. Email: yangxin_li@yahoo.com or Dr. Yan Xu, the Second Xiangya Hospital, Central South University, Changsha, Hunan, China. Email: xuyan217@csu.edu.cn. #These authors contributed equally to this work.

with preserved ejection fraction (HFpEF) [5]. Despite progress in the clinical management of CVDs, the fundamental molecular mechanisms driving cardiac aging remain incompletely understood, underscoring an urgent need for deeper mechanistic exploration.

A critical yet understudied dimension of aging is the decline in protein homeostasis (proteostasis). Cardiomyocytes, as terminally differentiated cells with very limited regenerative ability, rely heavily on accurate protein synthesis and rigorous quality control to maintain lifelong function [6, 7]. At the core of proteostasis lies the ribosome—the central machinery for protein production. Ribosome biogenesis is a tightly coordinated and energetically expensive process [8], and its dysregulation has increasingly been identified as a hallmark of aging [9, 10]. Age-related deterioration in ribosomal function and translation fidelity substantially contributes to the breakdown of proteostasis [11, 12], establishing ribosome biogenesis as a key frontier in deciphering age-related organ deterioration.

The nucleolus, the most prominent subnuclear compartment, functions as the assembly site for ribosomes [13]. Its structural and functional integrity is essential for cellular homeostasis, and its impairment has been associated with various human diseases, including cardiovascular disorders [14]. Nucleolin (Ncl) acts as a master regulator within the nucleolus, coordinating multiple stages of ribosome biogenesis—from rDNA transcription to rRNA processing and ribosomal subunit assembly [15, 16]. Beyond this fundamental role, Ncl has also been implicated in cardioprotection, modulating processes such as autophagy and cell proliferation [17, 18]. Nevertheless, its specific function and regulatory mechanisms in the setting of cardiac aging remain completely unexplored.

Meanwhile, the discovery of non-coding RNAs has fundamentally reshaped our understanding of gene regulation. Among these, circular RNAs (circRNAs)—a class of covalently closed RNA molecules—stand out due to their remarkable stability and growing recognition as potent regulatory agents [19-21]. circHIPK3, transcribed from the HIPK3 gene, is abundantly expressed in the heart and has been linked to roles in cell proliferation and cardiovascular pathology [22, 23]. Originally described as microRNA sponges, circRNAs are now understood to act through multiple mechanisms, such as directly interacting with mRNAs to influence their stability [24-26]. This functional versatility provides a compelling framework for investigating the mechanisms of circHIPK3. Beyond the regulatory roles of circRNAs, other layers of RNA metabolism, such as N^6-methyladenosine (m^6A) modification, have emerged as critical players in cardiac homeostasis and disease. For instance, m^6A methylation of RUNX1 mRNA enhances cytoskeleton remodeling and promotes cardiac fibrosis [27]. These findings underscore the multifaceted nature of RNA-based regulation in the heart and highlight the importance of integrating distinct RNA metabolic pathways to fully understand cardiac pathophysiology.

Furthermore, the functionality of the nucleolus is physically organized through liquid-liquid phase separation (LLPS), a process that drives the formation of biomolecular condensates [28, 29]. The aging process disrupts this delicate physicochemical balance, leading to aberrant condensate properties that impair ribosome production and promote cellular senescence [30]. Intriguingly, Nucleolin (Ncl) itself contains intrinsically disordered regions that facilitate its participation in LLPS [31], suggesting its function may be vulnerable to age-related phase separation defects. The potential intersection of a specific circRNA with the physical biology of the nucleolus represents a novel and unexplored axis in aging research.

In this study, we aim to investigate whether circHIPK3 expression is downregulated in the aging heart, and if so, whether it modulates cardiac aging through a novel mechanism involving direct stabilization of Ncl mRNA, thereby influencing Ncl-mediated LLPS dynamics and ribosome biogenesis.

MATERIALS AND METHODS

Plasmid and siRNA construction

Small interference RNA targeting circHIPK3 (circHIPK3 siRNA) was synthesized by Ribobio (Guangzhou, China). The sequence of circHIPK3 was amplified and cloned into a circRNA overexpression vector pK5ssAAV-ciR (Geneseed, Guangzhou, China) through restriction enzyme sites EcoRI and BamHI and confirmed by sequencing. The empty vector was used as negative control. After transfection for 40 h, H9C2 cells were harvested for subsequent experiments. Cells were transfected with plasmid or siRNA using Lipofectamine 2000 (Invitrogen, Carlsbad, CA, USA) according to the manufacturer's instructions.

Generation of circHIPK3 knockout mice

To avoid the confounding effects of estrogen, which is known to exert cardioprotective effects, only male mice were used in all aging-related experiments. To generate circHIPK3 knockout (CKO) mice, a construct was engineered for the disruption of circHIPK3, with two loxP sites flanking the downstream of short interspersed elements (SINEs) sequence of exon 2 of the HIPK3 gene. To engineer the targeting vector, homology arms and knockout region were generated by PCR using Bacterial

Artificial Chromosome (BAC) clone RP24-242C16 and RP24-245G14 from the C57BL/6 library as template. In the targeting vector, the Neo cassette was flanked by SDA (self-deletion anchor) sites. After the vector was linearized, ES cells were transfected by electroporation. Positive clones were selected by G418 treatment and verified by long-fragment PCR identification. Diphtheria toxin (DTA) was used for negative selection. Positive clones with correct homologous recombination were expanded and injected into blastocysts of C57BL/6J mice to obtain chimeric mice (circHIPK3$^{Flox/WT}$). The circHIPK3$^{Flox/WT}$ mice were generated by the Cyagen Biosciences Inc. The genotype of circHIPK3$^{Flox/Flox}$ mouse was confirmed by Sanger sequencing.

αMHC-driving CM-specific knockout mice were generated by crossing αMHC$^{Cre/WT}$ mice with circHIPK3$^{Flox/Flox}$ mice. The heterozygous αMHC$^{Cre/WT}$/ circHIPK3$^{Flox/WT}$ mice were back-crossed with the circHIPK3$^{Flox/Flox}$ mice to obtain CM-specific circHIPK3 CKO mice. The mouse genotype was identified by One Step Mouse Genotyping Kit (Vazyme, China). The CKO mice exhibited early cardiac senescence and cardiac dysfunction and the reproduction rate was very slow, suggesting that deletion of circHIPK3 impaired development. To overcome this problem, we generated inducible CM-specific circHIPK3 knockout (CKO) mice by crossing αMHC^{MerCreMer} mice with circHIPK3$^{Flox/Flox}$ mice. Induction of Cre recombinase activity was achieved using tamoxifen (Sigma, 100 μg/g body weight) dissolved in corn oil (Solarbio, China) and administrated intraperitoneally (i.p.). After tamoxifen administration, the hearts of CKO mice were harvested to confirm the deletion of circHIPK3.

Isolation of mouse cardiomyocytes (CMs)

Primary CMs were isolated from neonatal C57BL/6J mice as described previously. Briefly, the hearts were cut into small pieces (1-3 mm2), digested by 0.25% trypsin at 37°C, and the supernatant was collected into Dulbecco's modified Eagle's medium (DMEM) containing with 10% fetal bovine serum. After the tissue was completely digested, the supernatant was filtered through a cell strainer (100 μm) and then centrifuged at 1000 rpm for 5 min. The pellets were resuspended in DMEM containing 10% fetal bovine serum. The cells were seeded onto 10 cm plastic dishes for 2 h at 37°C to remove fibroblasts and then plated on 1% gelatin-coated plastic culture dishes.

Evaluation of cardiac function

Cardiac function was assessed *via* echocardiography using a 13 MHz transducer (VisualSonics). The left ventricular ejection fraction (EF) and fraction shortening (FS) were measured to evaluate heart performance.

Running endurance

Before running, mice were acclimated to the treadmill (Jiangsu SANS Biological Technology Co. Ltd.) for 1-3 h and to the motor sound for 15 min. The belt was initially set at a slow speed (6 m/min), then the velocity was increased 2 m every 2 min for the first 12 min and held steady (18 m/min). Exhaustion was defined as the point when mice spent more than 10 consecutive seconds on the shock grid without seeking to re-engage the treadmill.

Frailty assessment

Frailty was assessed in aged mice using an adapted Fried frailty phenotype. The frailty score (0-5) comprised five parameters: Weight loss: >5% loss over one week before endpoint (score 1); strength: Measured with a grip force meter; Treadmill endurance: Time to exhaustion on an accelerating treadmill; Gait speed: Time to traverse a corridor to a darkened box; Physical activity: Total distance traveled in an open field over 30 min.

For the four performance parameters, cutoff values were established as 1.5 SD below the mean of the most robust 50% control mice. Mice received 1 point for each parameter below cutoff or for weight loss exceeding 5%. Final scores categorized mice as robust (0), pre-frail (1-2), or frail (≥3).

EdU proliferation assay

Cell proliferation was evaluated using EdU Cell Proliferation Assay kit (Epizyme, Shanghai, China). Following various treatments, H9C2 cardiomyocytes were incubated in fresh medium containing 10 μM EdU for 2 h. Subsequently, H9C2 cells were washed with PBS, fixed with 4% paraformaldehyde for 30 min, and permeabilized with 0.5% Triton X-100 for 10 min. Cell nuclei were stained with DAPI for 15 minutes. The percentage of EdU-positive cells was then determined using fluorescence microscopy.

EU proliferation assay

Nascent RNA synthesis was evaluated using EU Cell Proliferation Assay kit (Epizyme, Shanghai, China). Following various treatments, H9C2 cardiomyocytes were incubated in fresh medium containing 10 μM EU for 2 h. Subsequently, H9C2 cells were washed with PBS, fixed with 4% paraformaldehyde for 30 min, and permeabilized with 0.5% Triton X-100 for 10 min. Cell nuclei were stained with DAPI for 15 minutes. The

percentage of EU-positive cells was then determined using fluorescence microscopy.

RNA extraction and real-time PCR

Total RNA was extracted using Trizol reagent (Takara). The extracted RNA was then reverse-transcribed into cDNA using the HiScript III RT reagent kit (Vazyme). Real-time PCR was performed with SYBR qPCR Master Mix (Vazyme) on the ABI (Foster City, CA, USA) StepOnePlus Real-Time PCR System. Primer sequences used for amplifications are listed in Supplementary Table S1.

GAPDH was used as the reference gene. Relative mRNA expression was normalized to GAPDH and presented as fold change relative to control group. The mRNA cycling conditions were as follows: an initial denaturation at 95°C for 30 s, followed by 40 cycles denaturation at 95°C for 5 s and annealing/extension at 60°C for 30 s. Each gene was analyzed in triplicate, and gene expression was calculated using the $2^{-\Delta\Delta Ct}$ method. All experiments were performed in triplicate to ensure reproducibility.

Western blot

Total proteins were extracted using RIPA buffer (Beyotime Biotechnology, China) and separated by SDS-polyacrylamide gel electrophoresis (SDS-PAGE), followed by transfer to polyvinylidene fluoride (PVDF) membranes (Millipore ISEQ00010). The membranes were initially incubated with primary antibodies, then with corresponding secondary antibodies. The antibodies used were: Nucleolin (14547) from Cell Signaling Technology (Danvers, MA, USA); RPL29 (Cat#15799-1-AP) from Proteintech Group (Chicago, IL, USA); GAPDH (Cat#AC002) from ABclonal (Wuhan, China); RPS3 (Cat#DF3684) from Affinity Biopharma (Shanghai, China); p21 (Cat#30427) from Signalway Antibody (Baltimore, MD, USA), puromycin (Cat#A23031) from ABclonal (Wuhan, China), IgG (H+L) (HRP-labeled Goat Anti-Rabbit IgG (H+L) (A0208) from Beyotime (Shanghai, China) and BeyoWB™ HRP-labeled Goat Anti-Mouse IgG (H+L) from Beyotime (Shanghai, China). Protein signals were detected using an ECL chemiluminescence kit (Biological Industries) and visualized on a BioRad luminescent imaging system. Relative protein expression was normalized to GAPDH and presented as fold change relative to control group.

Senescence-associated β-galactosidase (β-gal) staining

The β-gal staining was performed using senescence β-galactosidase staining kit (Beyotime Biotechnology, China) per manufacturer's instructions. In brief, neonatal primary cardiomyocytes were fixed at room temperature for 15 min, washed in PBS and stained in β-galactosidase solution at 37°C overnight. The number of positive cells was counted under a light microscope.

Telomere length assay

Genomic DNA was extracted using a tissue and blood DNA extraction kit (Tiangen Biotech, China) according to manufacturer's instructions. The single-copy gene 36B4 was used as a reference. The Ct values for the single-copy gene and telomere length were quantified using SYBR®Premix Ex Taq™. The T (telomere)/S (single-copy gene) ratio was ~[2Ct(telomere)/ 2Ct(36B4)]-1 (2-ΔCt), which reflected the relative length difference in telomeric DNA.

Ribosome-biogenesis AgNOR staining

Silver staining of NORs in control cells and Ncl siRNA treated cells were performed using standard AgNOR staining procedures. Briefly, following fixation, H9C2 cardiomyocytes or cardiac tissue sections were stained with freshly prepared AgNOR staining solution for 30 minutes. After staining, the samples were rinsed twice in ddH_2O and mounted for analysis. Images were captured using bright-field microscopy.

Immunofluorescence

Cells were fixed with 4% paraformaldehyde for 15 min, permeabilized with 0.5% Triton X-100 for 15 min, and blocked with 5% BSA for 30 min. Primary antibody was incubated overnight at 4°C, followed by Alexa Fluor-conjugated secondary antibody for 2 h at room temperature. Nuclei were counterstained with DAPI. Images were acquired using a confocal microscope. The antibodies used were: Nucleolin (14547) from Cell Signaling Technology (Danvers, MA, USA); Goat Anti-Rabbit IgG (Alexa Fluor®488) (ab150077) from Abcam (Cambridge, UK). Negative controls were performed by omitting the primary antibody or using isotype-matched IgG (A7016) from Beyotime (Shanghai, China). No specific staining was observed in these controls.

Ribo-Halo assay

The RPS3-HaloTag7 or RPL29-HaloTag7 donor plasmids, along with their respective gRNAs were designed and constructed by UBIGENE Biotechnology (Guangzhou, China). Briefly, 293T cells were seeded in 24-well plates and transfected with either the RPS3-HaloTag7 donor plasmid and its corresponding gRNA, or

the RPS29-HaloTag7 donor plasmid and gRNA, to generate Ribo-Halo cells. To label pre-existing ribosomes, 100 nM TMR-Halo ligand was added and incubated for 1 h. The cells were then washed with 1 mL of fresh DMEM and incubated for 5 min in the dark to remove the remaining excess TMR-ligand. Following this, the cells were transfected with Ncl siRNA and treated with 50 nM R110 Halo ligand for 24 h to label newly synthesized ribosomes. The proportion of labeled Halo- cells was analyzed using fluorescence microscopy.

Surface sensing of translation (SUnSET) assay

In vitro: H9C2 cells were transfected with indicated siRNAs or plasmids. After 48 h, cells were incubated with fresh medium containing puromycin (10 μg/mL) for 30 min at 37°C. Cells were then harvested, lysed in RIPA buffer, and subjected to Western blotting using an anti-puromycin antibody. GAPDH was used as a loading control.

In vivo: To assess global protein synthesis in the heart, mice were intraperitoneally injected with puromycin (0.04 μmol/g body weight). After 30 min, hearts were rapidly excised, rinsed in ice-cold PBS, and homogenized in RIPA buffer. Equal amounts of protein were analyzed by Western blotting with anti-puromycin antibody. GAPDH served as the loading control. Mice injected with PBS served as negative controls.

Ribo-disome assay

Cells grew to 70-80% confluency and treated with actidione for 10 min. After treatment, cells were washed with PBS and lysed in a lysis buffer. The lysates were then layered onto a 10%-35% sucrose gradients centrifuged at 40,000 rpm, 4°C for 2 h using a Beckmann Coulter ultracentrifuge. Ribosome profiles were assessed by measuring absorbance at 260 nm.

FRAP measurements

FRAP experiments were performed using a Zeiss LSM 880 confocal microscope with a 60×oil immersion objective. Ncl condensates were bleached with a 488 nm laser pulse, and fluorescence recovery was recorded for 180 s at 1 s intervals. Fluorescence intensities were analyzed using ZEN 3.8 software.

Recovery curves were fitted to a one-phase association model in GraphPad Prism. The recovery half-time ($t_{1/2}$), is defined as the time required for the fluorescence intensity to reach half of the final recovery level. And the diffusion coefficient was estimated using the Soumpasis model for a circular bleach spot.

LLPS assay in cells

H9C2 cells expressing Ncl-EGFP were cultured on coverslips. Once adhered, cells underwent two washes with PBS were fixed with 4% paraformaldehyde in PBS for 10 min. After two additional PBS washes, cells were examined using confocal microscopy (Zeiss, LSM 880). Ncl puncta were identified as visible puncta with a diameter greater than 0.5 μm.

CHIRP-qPCR

Following transfection of H9C2 cells with either the Ncl mRNA 5’ UTR wild-type plasmid or the Ncl mRNA 5' UTR mutant plasmid, cell lysates were co-incubated with circHIPK3 probes. DNA oligo probes, designed by RiboBio Biotechnology, contain BiotinTEG at 5’ end and target the back-splice junction of circHIPK3. Subsequent to transfection with the Ncl mRNA 5’ UTR plasmid, H9C2 cells were collected, crosslinked with 1% glutaraldehyde at room temperature for 10 min, and then reaction was quenched with 1.25 M glycine. Crosslinked cells underwent lysis and sonication. Chromatin was subjected to hybridization with biotinylated circHIPK3 probes at 37°C for 4 hours. Streptavidinconjugated beads (Invitrogen, Cat#65001) were introduced and incubated for 30 min. The precipitated RNA was subsequently identified and quantified through qPCR.

Statistical analysis

Statistical analyses were performed in GraphPad Prism 10.1. Replicates described in this study were treated as biological replicates. Quantitative data are presented as mean ± standard deviation (SD). Normality was assessed with the Shapiro-Wilk test. For data that did not meet normality assumptions or for groups with sample sizes $N < 6$, non-parametric alternatives were used (Mann-Whitney U test for two-group comparisons; and Kruskal-Wallis test followed by Dunn’s post hoc test with Bonferroni correction for multiple comparisons). For normally distributed data with appropriate sample sizes ($N \geq 6$), the unpaired two-tailed Student’s t-test was used for comparison between two groups. For comparisons among three or more groups, one-way ANOVA followed by Tukey’s post-hoc test was applied. Significance levels are indicated by p-values $p < 0.05$ (*), $p < 0.01$ (**), $p < 0.001$ (***). All procedures and analyses were performed by a researcher blinded to the treatment groups to ensure unbiased results.

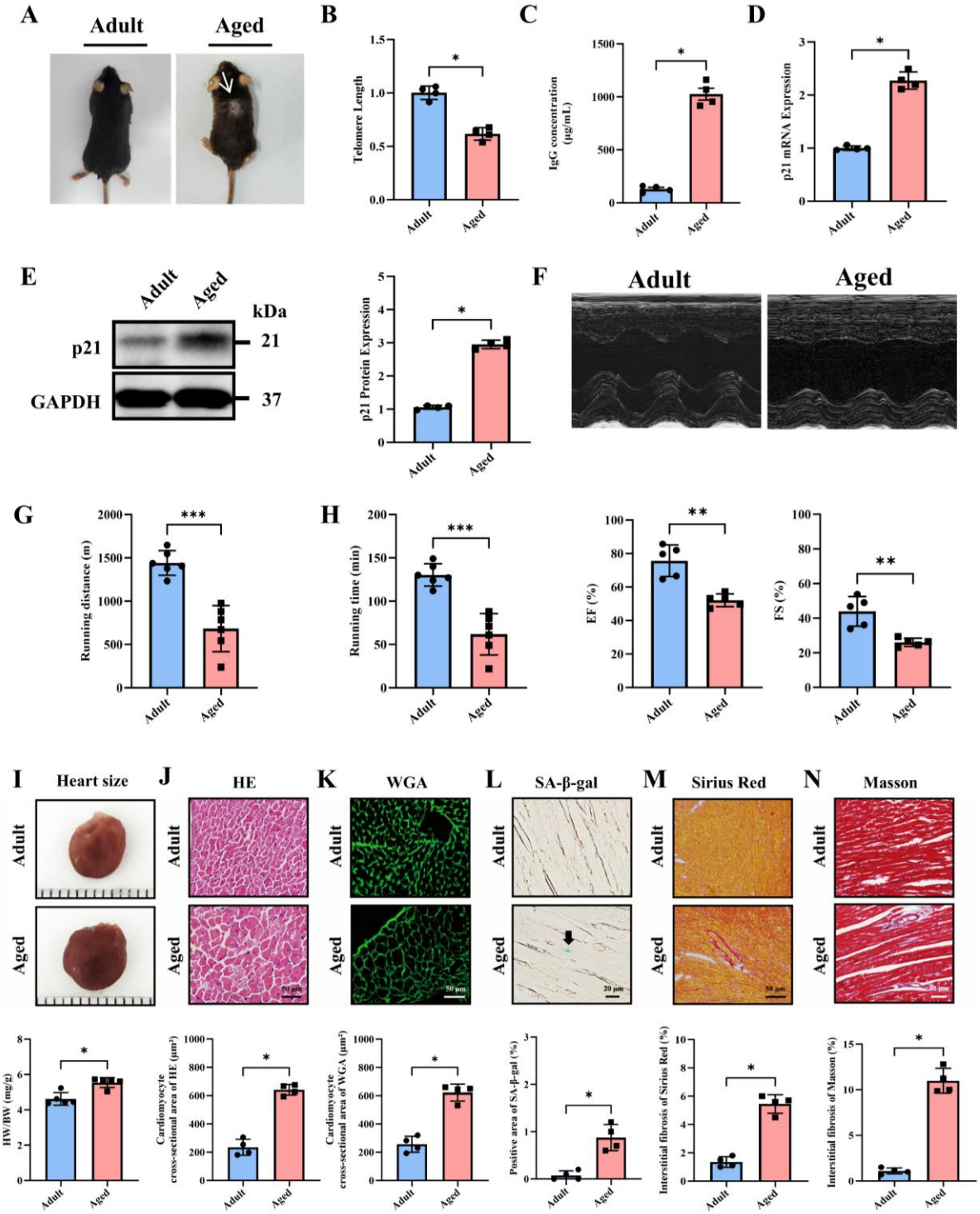

Figure 1. Age-related phenotypic alterations in the hearts of adult versus aged mice. (**A**) Representative appearance of Adult and Aged mice (n=6). (**B**) qRT-PCR was used to quantify relative telomere length in Adult and Aged mice heart tissues (n=4). (**C**) ELISA was used to detect IgG concentration in Adult and Aged mice myocardial interstitial fluid (n=4). (**D**) qRT-PCR was used to analyze p21 mRNA expression in Adult and Aged mice heart tissues (n=4). (**E**) Western blot was used to determine p21 protein level in Adult and Aged mice heart tissues (n=4). (**F**) Echocardiography was used to evaluate Adult and Aged mice cardiac function (n=5). (**G**) Treadmill exhaustion tests were used to assess running distance of Adult and Aged mice (n=6). (**H**) Treadmill exhaustion tests were used to measure running duration of Adult and Aged mice (n=6). (**I**) Visual observation was used to record heart size, and weighing was used to calculate the heart weight/body weight (HW/BW) ratio of

Adult and Aged mice (n=5). (**J, K**) HE staining and WGA fluorescent staining were used to quantify cardiomyocyte cross-sectional area of Adult and Aged mice (n=4). (**L**) SA-β-gal staining was performed on Adult and Aged mice heart (n=4). (**M, N**) Sirius Red staining and Masson's trichrome staining were used to quantify the fibrotic area fraction of Adult and Aged mice (n=4). (Mann-Whitney U test or Student's t-test). $p < 0.05$ (*), $p < 0.01$ (**), $p < 0.001$ (***).

RESULTS

Age-related phenotypic alterations in the hearts of aged mice

To characterize the physiological phenotypes of cardiac aging, we compared the hearts of young adult (4-6 months old) and naturally aged (20-24 months old) male mice. Aged mice exhibited focal alopecia (Fig. 1A). At the molecular level, cardiac aging was confirmed by significantly shortened telomere length in aged hearts (Fig. 1B) and increased accumulation of IgG—a marker of aging-related tissue dysfunction (Fig. 1C). Consistent with these findings, the expression of p21 was markedly upregulated at both mRNA and protein levels in aged hearts (Fig. 1D, E). Functional assessment by echocardiography revealed reduced left ventricular ejection fraction (EF) and fractional shortening (FS), indicating impaired cardiac contractile function (Fig. 1F). Meanwhile, treadmill tests demonstrated that aged mice exhibited significantly decreased running distance and duration compared to young controls (Fig. 1G, H).

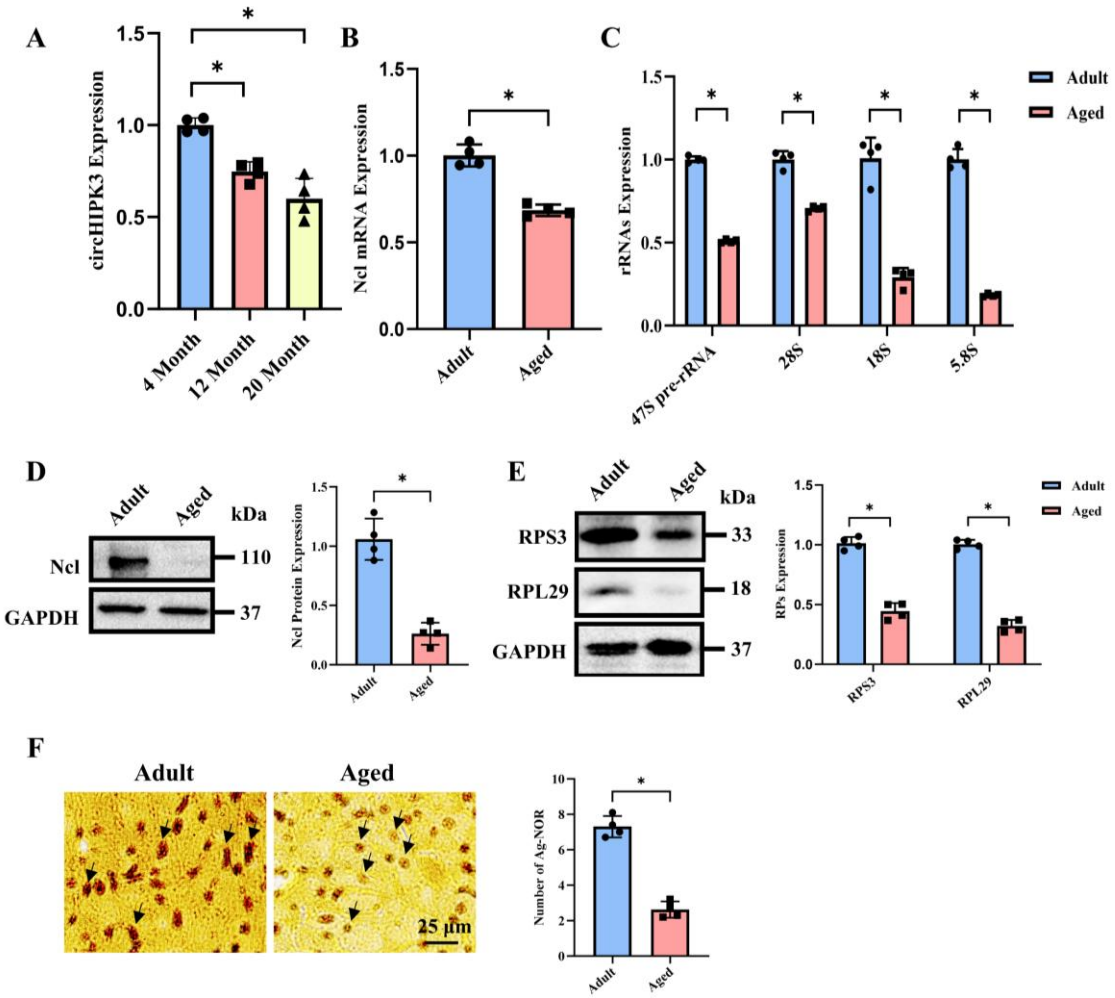

Figure 2. Age-related changes in circHIPK3 expression, Ncl levels, and ribosome biogenesis indices in mice. (**A**) qRT-PCR was used to quantify circHIPK3 expression in 4-month-old (4M), 12-month-old (12M), and 20-month-old (20M) mouse heart tissues (n=4). (**B**) qRT-PCR was used to analyze Ncl mRNA expression in Adult and Aged mice heart tissues (n=4). (**C**) qRT-PCR was used to detect the expression of rRNAs in Adult and Aged mice heart tissues (n=4). (**D**) Western blot was used to determine Ncl protein level in Adult and Aged mice heart tissues (n=4). (**E**) Western blot was used to measure RPS3 and RPL29 protein levels in Adult and Aged mice heart tissues (n=4). (**F**) Ag-NOR staining was used to detect ribosome biogenesis in Adult and Aged mice cardiomyocytes (n=4). (Mann-Whitney U test or Kruskal-Wallis test). $p < 0.05$ (*), $p < 0.01$ (**), $p < 0.001$ (***).

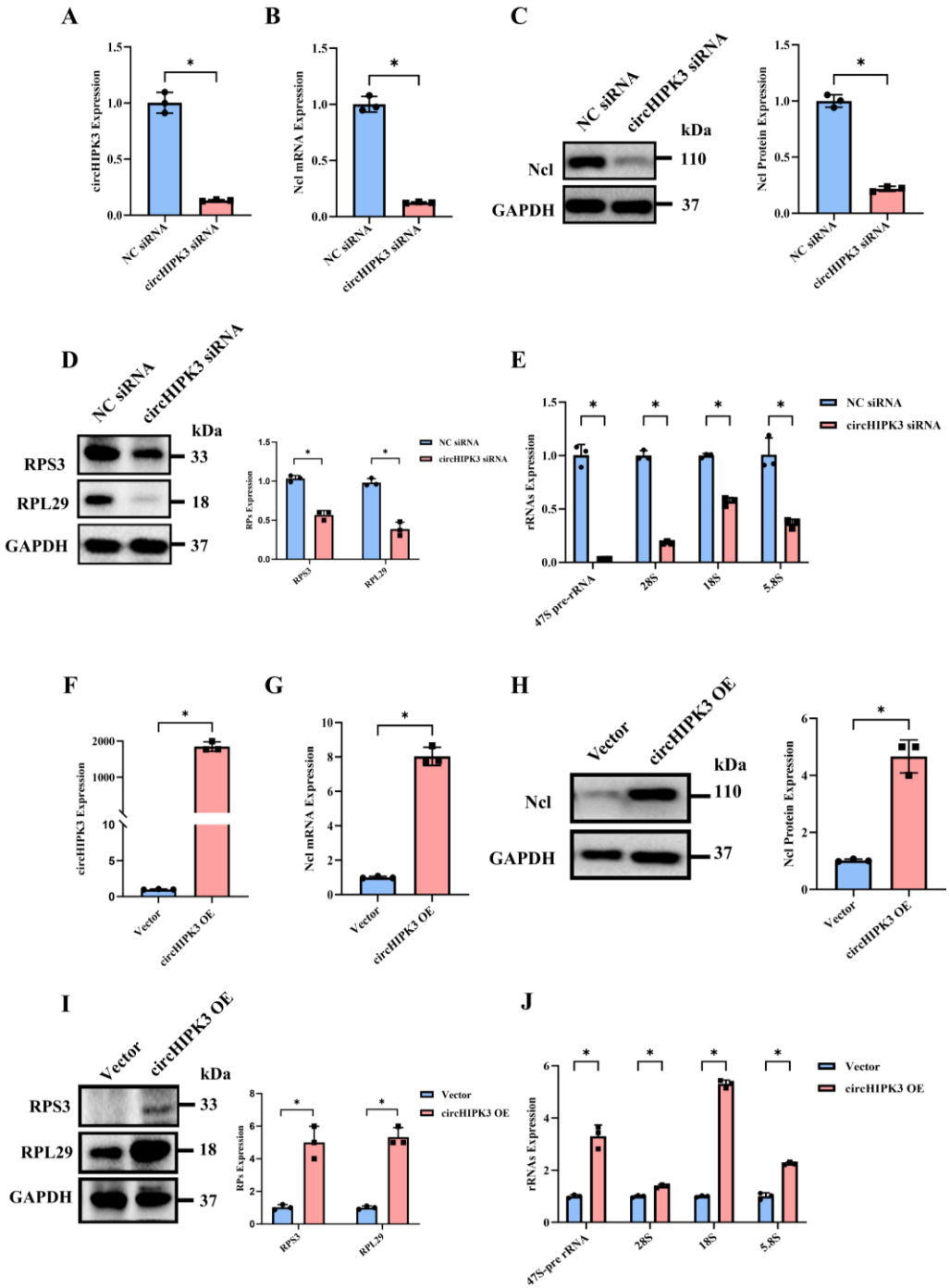

Figure 3. circHIPK3 regulates Ncl and ribosomal protein expression. (**A**) qRT-PCR was used to detect circHIPK3 expression in H9C2 cells after siRNA transfection (n=3). (**B**) qRT-PCR was used to analyze Ncl mRNA expression in H9C2 cells after siRNA transfection (n=3). (**C**) Western blot was used to determine Ncl protein level in H9C2 cells after siRNA transfection (n=3) (**D**) Western blot was used to measure RPS3 and RPL29 protein levels in H9C2 cells after siRNA transfection (n=3). (**E**) qRT-PCR was used to detect the expression of rRNAs in H9C2 cells after siRNA transfection (n=3). (**F**) qRT-PCR was used to detect circHIPK3 expression in H9C2 cells after transfection of overexpression plasmid (n=3). (**G**) qRT-PCR was used to detect Ncl mRNA expression in H9C2 cells after transfection of overexpression plasmid (n=3). (**H**) Western blot was used to determine Ncl protein level in H9C2 cells after transfection of overexpression plasmid (n=3). (**I**) Western blot was used to measure RPS3 and RPL29 protein levels in H9C2 cells after transfection of overexpression plasmid (n=3). (**J**) qRT-PCR was used to detect the expression of rRNAs in H9C2 cells after transfection of overexpression plasmid (n=3). (Mann-Whitney U test). $p < 0.05$ (*), $p < 0.01$ (**), $p < 0.001$ (***).

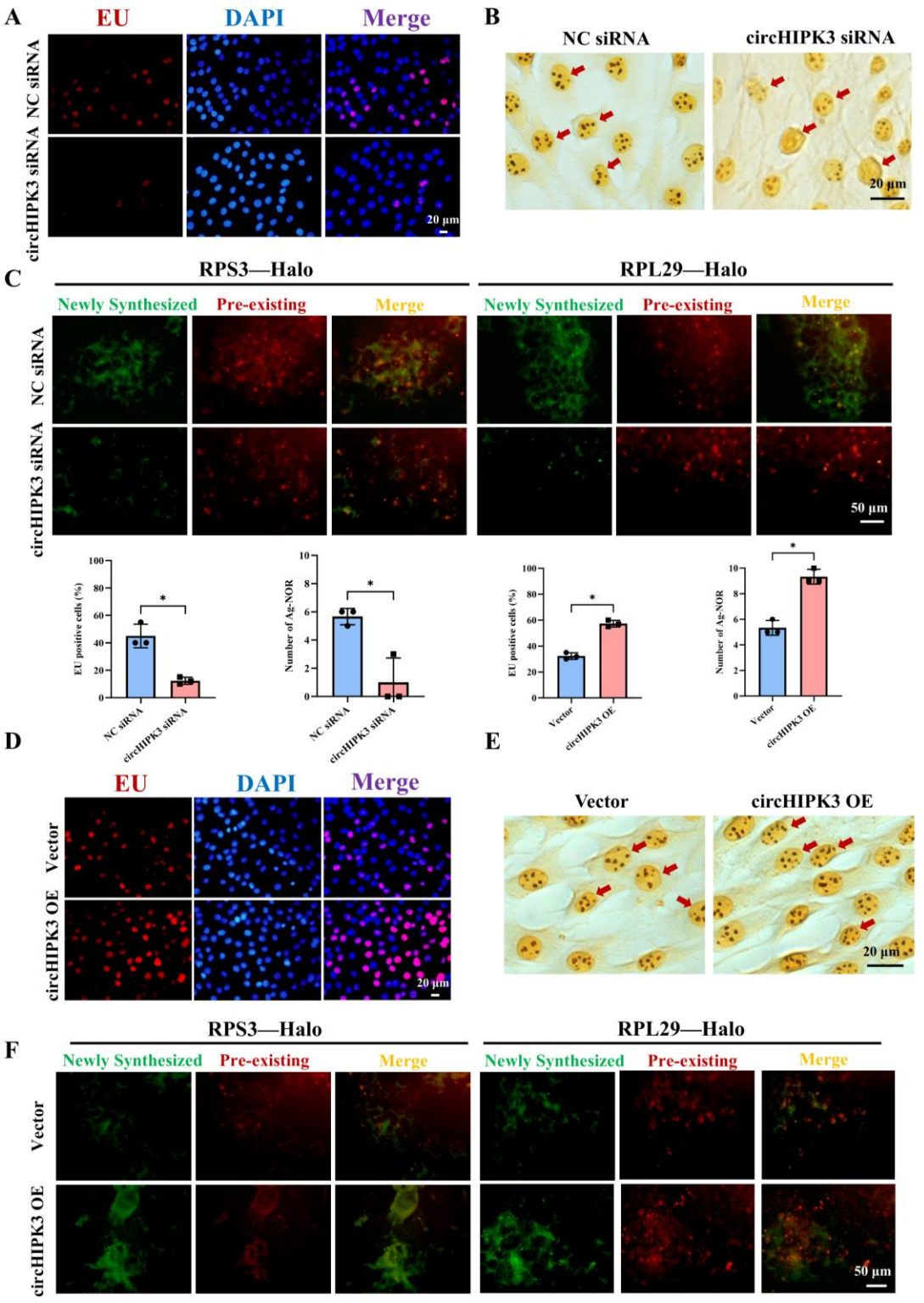

Figure 4. circHIPK3 deficiency impairs ribosome biogenesis. (**A-C**) EU incorporation, Ag-NOR staining and Ribo-Halo were performed to detect ribosome biogenesis in H9C2 cells after siRNA transfection (n=3). (**D-F**) EU incorporation, Ag-NOR staining and Ribo-Halo were performed to detect ribosome biogenesis in H9C2 cells after transfection of overexpression plasmid (n=3). Representative images were selected from at least three independent experiments and data were presented. (Mann-Whitney U test). $p < 0.05$ (*), $p < 0.01$ (**), $p < 0.001$ (***).

Structurally, aged mice exhibited an increased heart weight-to-body weight ratio (Fig. 1I), accompanied by features of cardiac hypertrophy, as indicated by an enlarged cardiomyocyte cross-sectional area in HE staining and WGA staining (Fig. 1J, K). Furthermore, aged hearts showed increased SA-β-Gal positivity (Fig. 1L) and a greater fibrotic area, as detected by Masson's trichrome staining and Sirius Red staining (Fig. 1M, N). Taken together, these findings demonstrate that aged mouse hearts exhibit typical aging-related phenotypes, encompassing functional decline, structural remodeling, cellular senescence, and fibrosis.

Identification of circHIPK3 as a key regulatory RNA governing ribosome biogenesis during murine cardiac aging

To identify key regulators of cardiac aging, we first screened for cardiac-enriched circular RNAs and focused on circHIPK3, which is highly conserved and abundant in the heart (Supplemntary Fig. 1A). qRT-PCR analysis of hearts from 4-month-old, 12-month-old, and 20-month-old mice revealed a progressive age-dependent downregulation of circHIPK3 expression, which decreased to approximately 60% of the level observed in young mice (Fig. 2A).

Given the critical role of ribosome biogenesis in proteostasis and aging, we analyzed GEO RNA-sequencing data of young and aged mouse hearts (GEO accession number: GSE8146) [32], revealing that Ncl and multiple ribosomal protein genes were significantly downregulated in aged hearts (Supplemntary Fig. 1B, C). qRT-PCR validation confirmed decreased mRNA levels of Ncl, and rRNAs in aged hearts (Fig. 2B, C). Western blot analysis further verified reduced protein expression of Ncl, ribosomal proteins RPS3 and RPL29 in aged hearts (Fig. 2D, E). Silver staining of argyrophilic nucleolar organizing regions (Ag-NORs) showed that aged hearts had fewer Ag-NORs per cell, indicating impaired ribosome biogenesis (Fig. 2F). These results identify circHIPK3 as a potential key regulatory RNA that correlates with Ncl expression, ribosome biogenesis, and murine cardiac aging.

circHIPK3 regulates Ncl and ribosomal protein expression

To validate the functional role of circHIPK3, we silenced or overexpressed circHIPK3 in H9C2 cells and mouse primary cardiomyocytes (Supplementary Table 2, Supplemntary Fig. 1D). Importantly, cirSupplentary FcHIPK3 knockdown did not affect linear HIPK3 mRNA levels (Supplemntary Fig. 1E). Silencing circHIPK3 significantly reduced the mRNA and protein levels of Ncl, ribosomal proteins RPS3 and RPL29 (Fig. 3A-D), as well as a decrease in rRNA synthesis in H9C2 cells (Fig. 3E), while overexpressing circHIPK3 had the opposite effect (Fig. 3F-J).

circHIPK3 deficiency impairs ribosome biogenesis

We next assessed the functional consequences of circHIPK3 modulation on ribosome biogenesis. Functional assays demonstrated that circHIPK3 deficiency inhibited ribosome biogenesis: 5-ethynyluridine (EU) incorporation was decreased (Fig. 4A), Ag-NOR numbers were reduced (Fig. 4B), and Ribo-Halo assays showed impaired ribosome production (Fig. 4C, Supplemntary Fig. 1F). Conversely, circHIPK3 overexpression enhanced EU incorporation (Fig. 4D), Ag-NOR numbers (Fig. 4E), and de novo ribosome synthesis (Fig. 4F, Supplemntary Fig. 1G).

circHIPK3 deficiency elicits senescence in cardiomyocytes

Beyond ribosome biogenesis defects, circHIPK3 deficiency directly drove cardiomyocyte senescence, while its overexpression attenuated senescent phenotypes. p21 expression was assessed via qRT-PCR and Western blot: silencing circHIPK3 in H9C2 cells and primary cardiomyocytes significantly upregulated p21 protein and mRNA levels, whereas circHIPK3 overexpression reduced p21 expression at both transcript and protein levels (Fig. 5A-D).

Consistent with p21 changes, SA-β-Gal staining showed that circHIPK3-silenced primary cardiomyocytes exhibited a increase in SA-β-Gal-positive cells (Fig. 5E). In contrast, circHIPK3 overexpression decreased the SA-β-Gal-positive rate, confirming circHIPK3's anti-senescence role (Fig. 5F).

To link senescence to functional impairment, we evaluated cardiomyocyte proliferation via EdU incorporation assays. Silencing circHIPK3 reduced EdU-positive cells, indicating blunted proliferation (Fig. 5G). Conversely, circHIPK3 overexpression elevated EdU-positive cells, restoring proliferative capacity (Fig. 5H).

circHIPK3 regulates Ncl LLPS to maintain ribosome biogenesis

Nucleolar function relies on LLPS of key proteins such as Ncl. Bioinformatics analysis predicted that Ncl contains intrinsic disordered regions (IDRs) — a structural feature enabling LLPS (Supplemntary Fig. 2A, B). Immunofluorescence staining showed that silencing circHIPK3 altered Ncl' size, form, quantity and fluorescence intensity in H9C2 cells: Ncl formed larger,

irregular aggregates with reduced fluorescence intensity compared to the small, uniform puncta in control cells (Fig. 6A-D).

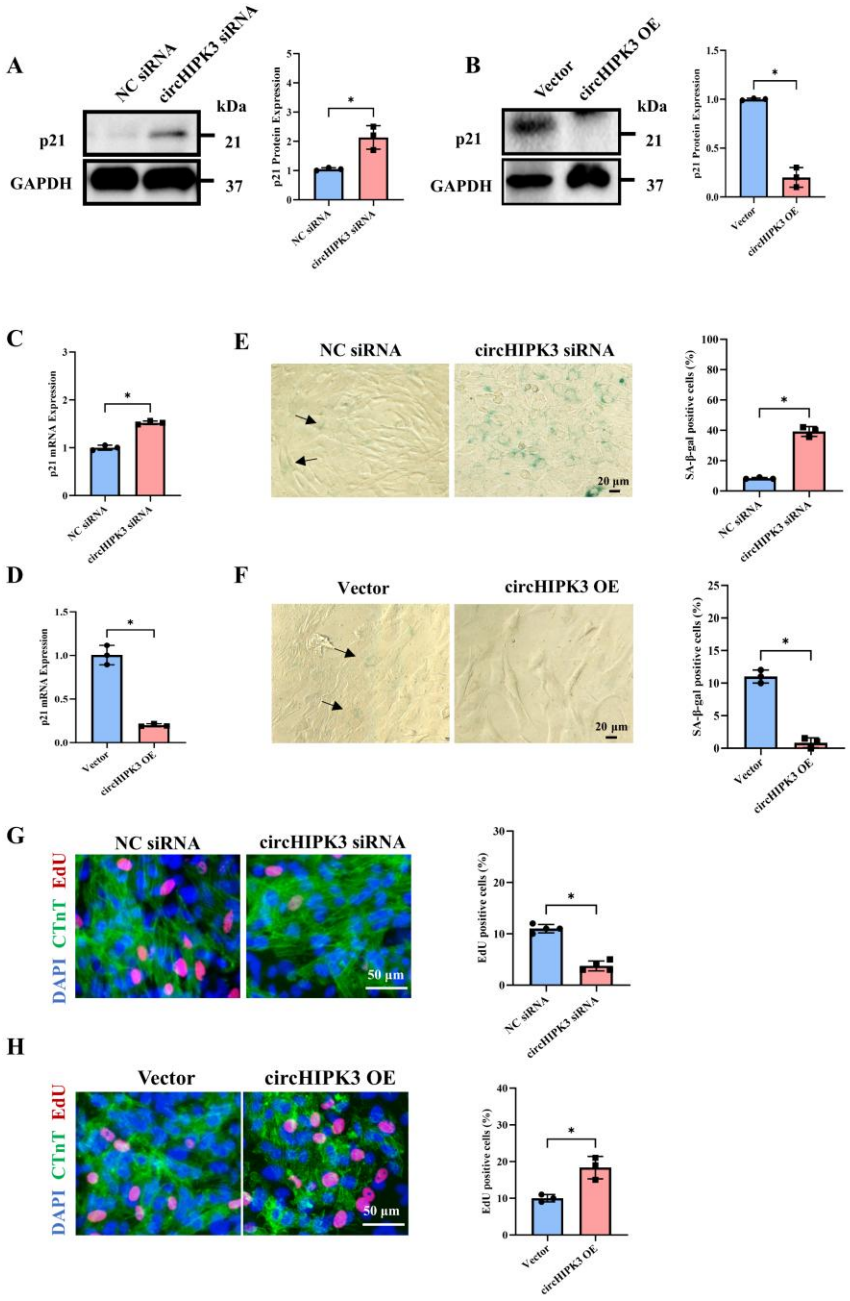

Figure 5. Effects of circHIPK3 knockdown and overexpression on cellular senescence and proliferation in cells. (**A**) Western blot was used to determine p21 protein level in H9C2 cells after siRNA transfection (n=3). (**B**) Western blot was used to determine p21 protein level in H9C2 cells after transfection of overexpression plasmid (n=3). (**C**) qRT-PCR was used to analyze p21 mRNA expression in H9C2 cells after siRNA transfection (n=3). (**D**) qRT-PCR was used to analyze p21 mRNA expression in H9C2 cells after transfection of overexpression plasmid (n=3). (**E**) SA-β-gal staining was performed to detect senescent cells in H9C2 cells after siRNA transfection (n=3). (**F**) SA-β-gal staining was performed to detect senescent cells in H9C2 cells after transfection of overexpression plasmid (n=3). (**G**) EdU incorporation assay was performed to evaluate cell proliferation in primary cardiomyocytes after siRNA transfection (n=3). (**H**) EdU incorporation assay was performed to evaluate cell proliferation in primary cardiomyocytes after transfection of overexpression plasmid (n=3). (Mann-Whitney U test). $p < 0.05$ (*), $p < 0.01$ (**), $p < 0.001$ (***).

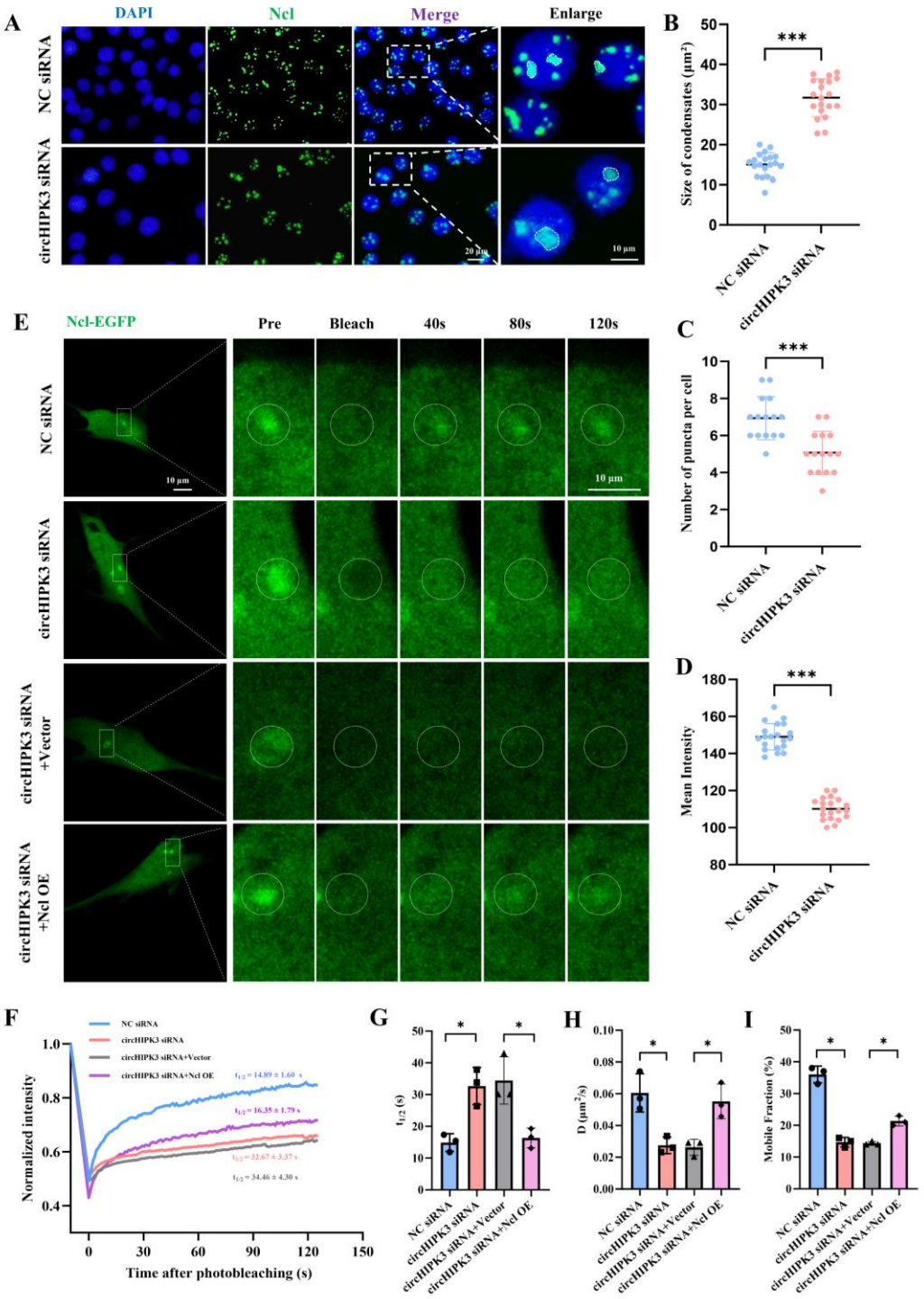

Figure 6. Ncl LLPS is impaired upon circHIPK3 deficiency. (**A**) Immunofluorescence analysis of Ncl distribution in H9C2 cells (n=4). (**B**) Quantification of the average size of Ncl puncta (n=20, each dot represents an individual cell from three independent experiments). (**C**) The number of Ncl puncta per cell (n=15, each dot represents an individual cell from three independent experiments). (**D**) Quantification of the mean fluorescence intensity of Ncl puncta (n=20, each dot represents an individual cell from three independent experiments). (**E**) Representative images from FRAP assays assessing LLPS capacity of Ncl (n=3). (**F**) FRAP recovery curves of Ncl-EGFP condensates under indicated conditions (n=3). (**G**) Quantification of recovery half-time ($t_{1/2}$) (n=3). (**H**) Quantification of diffusion coefficient (D) (n=3). (**I**) Quantification of the mobile fraction (n=3). Representative images were selected from at least three independent experiments and data were presented. (Student's t-test or Mann-Whitney U test or Kruskal-Wallis test). $p < 0.05$ (*), $p < 0.01$ (**), $p < 0.001$ (***).

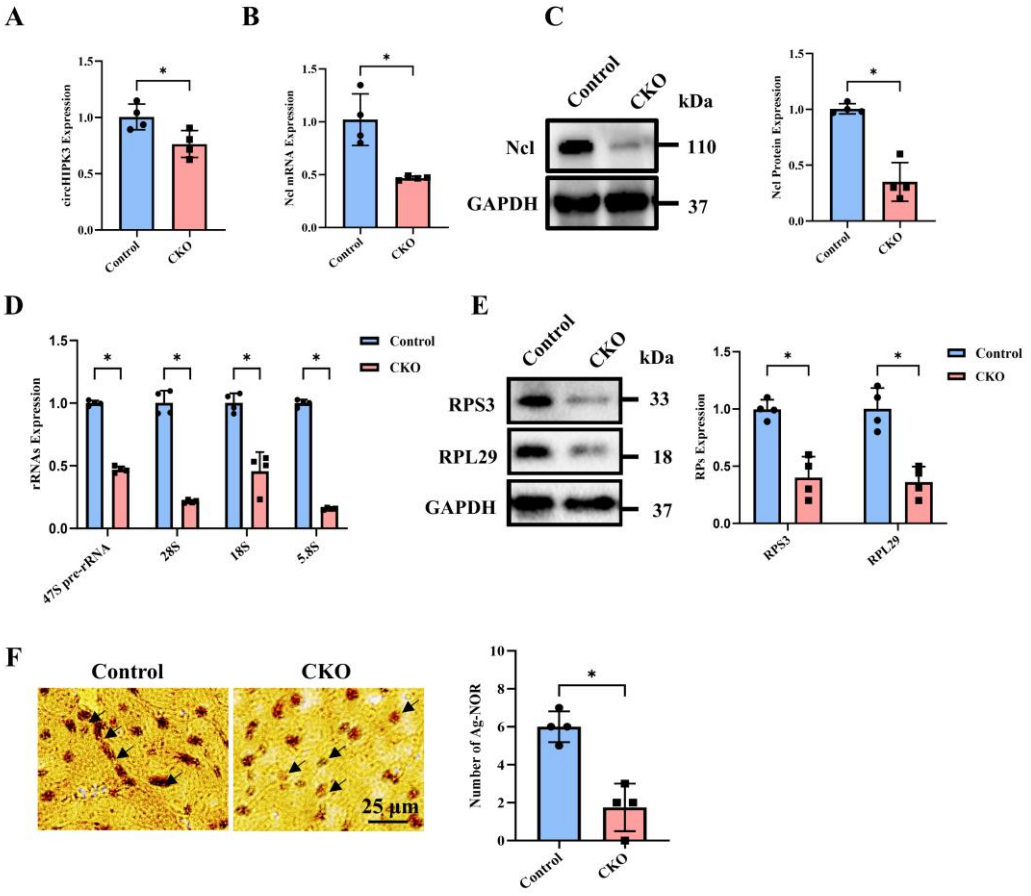

Figure 7. Effects of cardiomyocyte-specific circHIPK3 knockout (CKO) on ribosome biogenesis in mice. (A) qRT-PCR was used to analyze circHIPK3 mRNA expression in Control and CKO mice heart tissues (n=4). (**B**) qRT-PCR was used to analyze Ncl mRNA expression in Control and CKO mice heart tissues (n=4). (**C**) Western blot was used to determine Ncl protein level in Control and CKO mice heart tissues (n=4). (**D**) qRT-PCR was used to analyze rRNAs expression in Control and CKO mice heart tissues (n=4). (**E**) Western blot was used to measure RPS3 and RPL29 protein levels in Control and CKO mice heart tissues (n=4). (**F**) Ag-NOR staining was performed to detect ribosome biogenesis in Control and CKO mice heart tissues (n=4). (Mann-Whitney U test). $p < 0.05$ (*), $p < 0.01$ (**), $p < 0.001$ (***).

FRAP assays were performed to quantify Ncl LLPS dynamics. In control cells, bleached Ncl puncta recovered substantial fluorescence, indicating high molecular mobility. In contrast, circHIPK3-silenced cells showed minimal fluorescence recovery (Fig. 6E). Moreover, FRAP assays further demonstrated that circHIPK3 knockdown prolonged the recovery half-time ($t_{1/2}$) and reduced the diffusion coefficient (D) and mobile fraction. Remarkably, Ncl overexpression restored all three parameters to near-control levels (Fig.6F-I). These data indicate that circHIPK3 is required for supporting normal Ncl LLPS dynamics, and its deficiency is associated with altered Ncl phase separation behavior, a defect that contributes to impaired ribosome biogenesis.

Cardiomyocyte-specific knockout of circHIPK3 impairs ribosome biogenesis *in vivo*

To confirm the *in vivo* role of circHIPK3 in ribosome biogenesis, we generated cardiomyocyte-specific circHIPK3 knockout (CKO) mice using the Cre-loxP system, with induction by tamoxifen injection in 8-week-old mice (Supplemntary Fig. 2C, D, E). qRT-PCR confirmed efficient knockdown of circHIPK3 in CKO hearts, while the expression of linear HIPK3 mRNA remained unchanged (Fig. 7A, S2F). To exclude potential developmental effects of circHIPK3 deletion, we assessed cardiac morphology and function in all mice prior to tamoxifen induction. Echocardiographic analysis revealed no significant differences between Control and CKO mice in baseline cardiac function or structural parameters (Supplemntary Fig. 3A-G). These data confirm that the observed aging phenotypes in CKO mice result from adult-onset circHIPK3 deletion, rather than pre-existing developmental abnormalities.

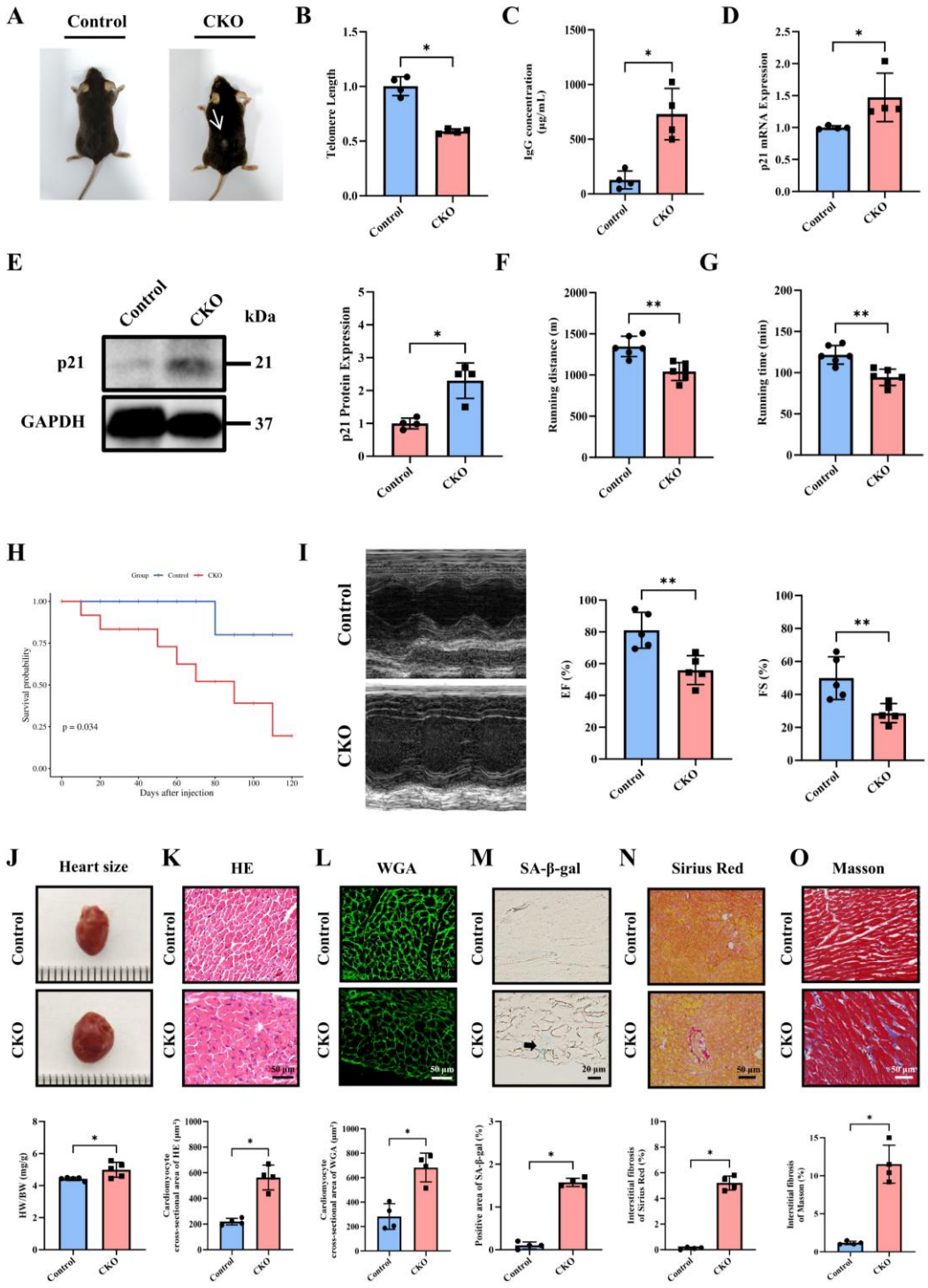

Figure 8. Effects of cardiomyocyte-specific circHIPK3 knockout (CKO) on senescence and survival in mice. (**A**) Representative appearance of Control and CKO mice (n=6). (**B**) qRT-PCR was used to quantify relative telomere length in Control and CKO mice heart tissues (n=4). (**C**) ELISA was used to detect IgG concentration in Control and CKO mice myocardial interstitial fluid (n=4). (**D**) qRT-PCR was used to analyze p21 mRNA expression in Control and CKO heart tissues (n=4). (**E**) Western blot was used to determine p21 protein level in Control and CKO mice heart tissues (n=4). (**F**) Treadmill exhaustion tests were used to assess running distance of Control and CKO mice (n=6). (**G**) Treadmill exhaustion tests were used to measure running duration of Control and CKO mice (n=6). (**H**) Curve was used to evaluate the survival probability of Control and CKO mice (n=20 per group). (**I**) Echocardiography was used to evaluate Control and CKO mice cardiac function (n=5). (**J**) Visual observation was used to record heart size, and

weighing was used to calculate the heart weight/body weight (HW/BW) ratio of Control and CKO mice (n=5). (**K, L**) HE staining and WGA fluorescent staining were used to quantify cardiomyocyte cross-sectional area of Control and CKO mice (n=4). (**M**) SA-β-gal staining was performed on Control and CKO mice heart (n=4). (**N, O**) Sirius Red staining and Masson's trichrome staining were used to quantify the fibrotic area fraction of Control and CKO mice (n=4). (Mann-Whitney U test). $p < 0.05$ (*), $p < 0.01$ (**), $p < 0.001$ (***).

Consistent with *in vitro* findings, CKO hearts exhibited significantly reduced mRNA and protein levels of Ncl (Fig. 7B, C), along with decreased expression of rRNAs (Fig. 7D) and ribosomal proteins RPS3 and RPL29 (Fig. 7E). Furthermore, Ag-NOR staining revealed a marked reduction in the number of Ag-NORs per nucleus in CKO cardiomyocytes, indicating impaired ribosome biogenesis (Fig. 7F). Collectively, these results demonstrate that cardiomyocyte-specific deletion of circHIPK3 disrupts the ribosome biogenesis pathway *in vivo*, recapitulating the molecular defects observed in aged hearts.

Cardiomyocyte-specific knockout of circHIPK3 recapitulates systemic and cardiac aging phenotypes

Beyond ribosome biogenesis defects, CKO mice exhibited pronounced systemic and cardiac aging phenotypes. Systemically, CKO mice showed developed focal alopecia (Fig. 8A). At the molecular level, cardiac tissues from CKO mice displayed shortened telomere length (Fig. 8B), increased accumulation of IgG (Fig. 8C), and upregulated expression of the senescence marker p21 at both mRNA and protein levels (Fig. 8D, E).

Functionally, CKO mice demonstrated significant exercise intolerance, with reduced running distance and duration in treadmill tests (Fig. 8F, G) and showed reduced survival probability (Fig. 8H). Echocardiography revealed impaired cardiac contractility, as evidenced by decreased ejection fraction (EF) and fractional shortening (FS) (Fig. 8I). Structurally, CKO hearts exhibited increased heart weight-to-body weight ratio (Fig. 8J), cardiomyocyte hypertrophy (Fig. 8K, L), enhanced SA-β-Gal activity (Fig. 8M), and elevated cardiac fibrosis (Fig. 8N, O). These phenotypes closely mirror those observed in naturally aged mice, confirming that cardiomyocyte-specific loss of circHIPK3 is sufficient to drive comprehensive cardiac aging *in vivo*.

circHIPK3 stabilizes Ncl mRNA via direct interaction to counteract cardiac aging

To elucidate the molecular mechanism by which circHIPK3 regulates Ncl, we first examined the subcellular localization of circHIPK3 via cellular fractionation and qRT-PCR analysis. The results showed that circHIPK3 was predominantly localized in the cytoplasm of cardiomyocytes, which is consistent with its potential role in post-transcriptional regulation (Fig. 9A). Given the cytoplasmic localization, we hypothesized that circHIPK3 might directly interact with Ncl mRNA. Bioinformatics prediction using RNAhybrid software revealed complementary base-pairing motifs between circHIPK3 and the 5' UTR of Ncl mRNA (Fig. 9B, C). ChIRP-qPCR assays confirmed direct binding between circHIPK3 and the 5' UTR of Ncl mRNA in cardiomyocytes; this binding was abrogated when the 5' UTR was mutated (Fig 9D, S2G, Supplementary Table S3). Next, we investigated whether circHIPK3 regulates Ncl mRNA stability. Cardiomyocytes transfected with si-circHIPK3 or control siRNA were treated with actinomycin D (ActD) to inhibit de novo transcription. The results showed that the stability of Ncl mRNA was significantly decreased upon circHIPK3 knockdown (Fig. 9E). To serve as a negative control, the stability of GAPDH mRNA was not affected (Fig. 9F). Collectively, these data demonstrate that circHIPK3 directly binds to the 5' UTR of Ncl mRNA to enhance its stability, thereby regulating Ncl expression in cardiomyocytes.

Ncl overexpression rescues circHIPK3 deficiency-induced ribosome biogenesis defects and senescence in H9C2 cells

To determine whether Ncl mediates the functional effects of circHIPK3, we performed rescue experiments by overexpressing Ncl in circHIPK3-deficient cardiomyocytes. We first assessed global translation rates using SUnSET assays. The results showed that the decreased translation activity caused by circHIPK3 knockdown was significantly rescued by Ncl overexpression (Fig. 10A, B, S2H). EU incorporation assays further revealed that the reduced nascent rRNA synthesis in circHIPK3-deficient cells was restored upon Ncl overexpression (Fig. 10C). Polysome profiling analysis demonstrated that the accumulation of disomes observed in si-circHIPK3 cells was reversed to a normal distribution after Ncl overexpression (Fig. 10D). We next examined cellular senescence markers. SA-β-gal staining showed that the increased percentage of senescent cells induced by circHIPK3 knockdown was significantly reduced by Ncl overexpression (Fig. 10E). In line with this, p21 protein levels returned to near-control levels upon Ncl rescue (Fig. 10F).

Collectively, these results demonstrate that Ncl overexpression is sufficient to rescue the translational dysfunction, ribosome biogenesis defects, and cellular senescence caused by circHIPK3 deficiency.

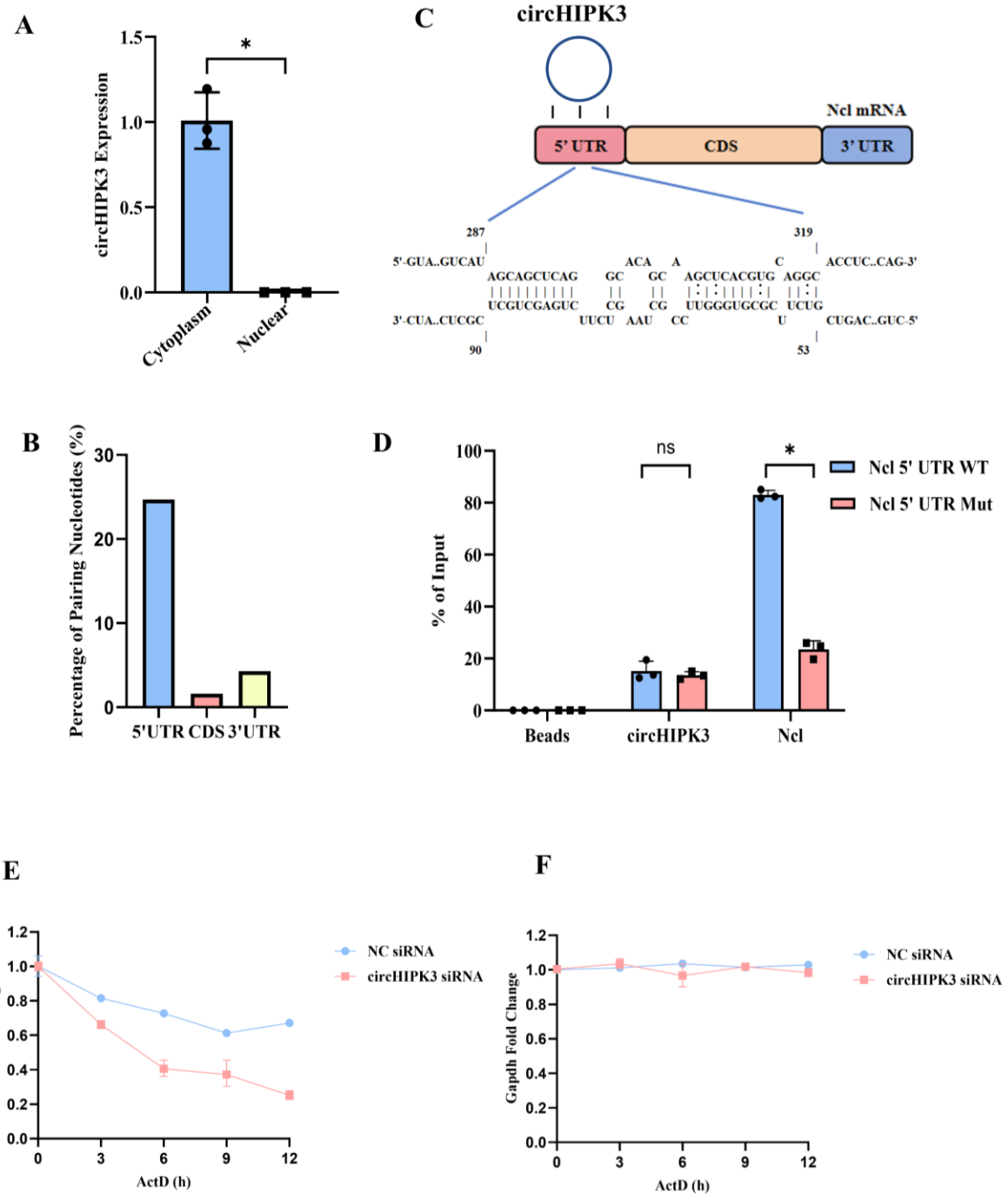

Figure 9. circHIPK3 pairs with the 5' UTR of Ncl mRNA to stabilize Ncl mRNA. (**A**) Nuclear-cytoplasmic fractionation combined with qRT-PCR was used to detect circHIPK3 expression levels in the cytoplasm and nucleus (n=3). (**B**) The density of circHIPK3 binding sites in the designated regions of Ncl mRNA. (**C**) Bioinformatics prediction using the RNAhybrid data base revealed that circHIPK3 has a continuous binding site with the 5' UTR of Ncl mRNA. (**D**) ChIRP-qPCR was used to detect the binding between circHIPK3 and Ncl mRNA in H9C2 cells (n=3). (**E, F**) H9C2 cells were transfected with NC siRNA or circHIPK3 siRNA and then treated with or without Actinomycin D (ActD, 10 μg/mL) for duration as indicated, followed by qRT-PCR analysis to examine the expression of Ncl (E) and GAPDH (F) (n=3). (Mann-Whitney U test or Kruskal-Wallis test). $p < 0.05$ (*), $p < 0.01$ (**), $p < 0.001$ (***).

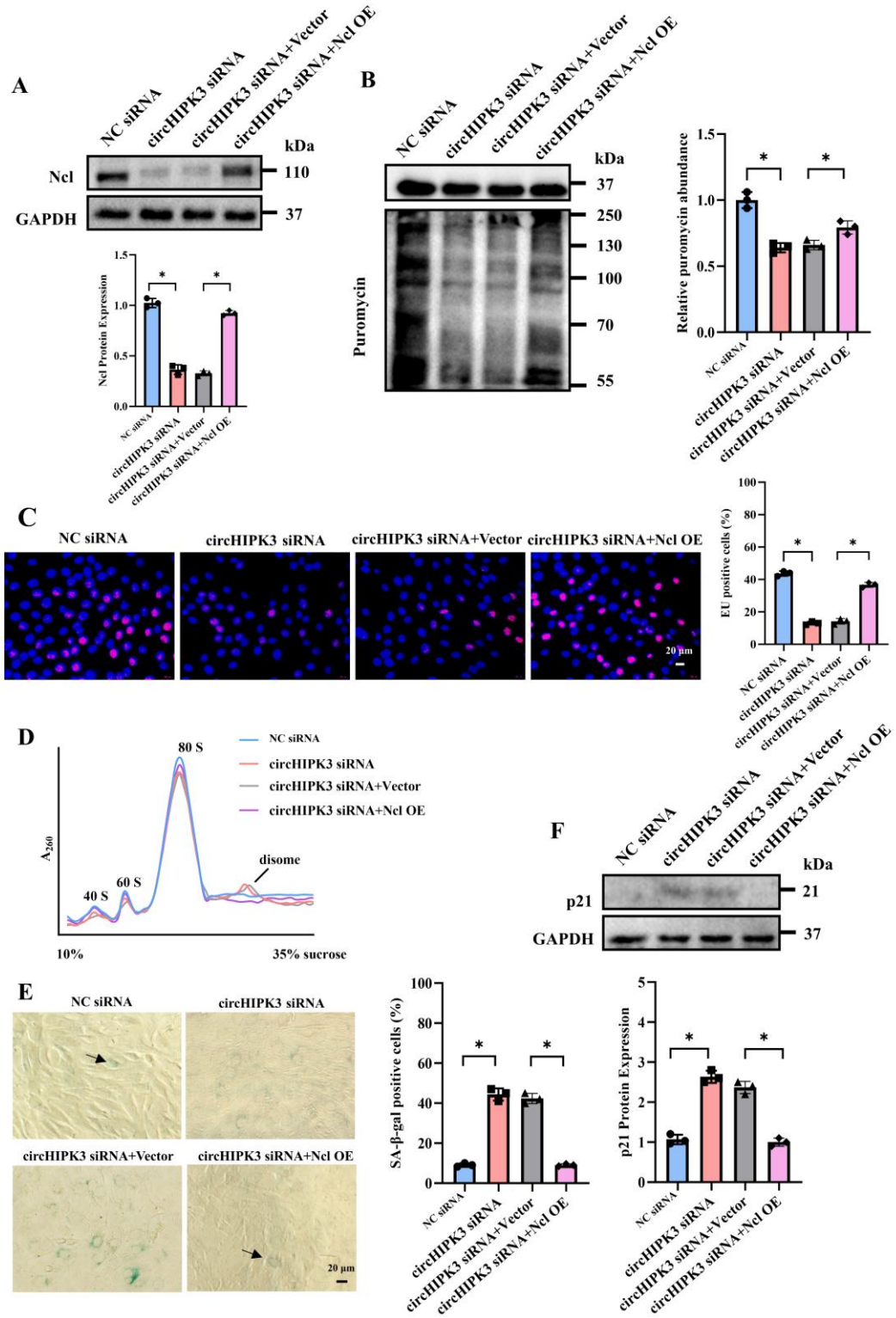

Figure 10. Ncl restoration rescues circHIPK3 deficiency-induced translational and senescence defects in H9C2 cells. (**A**) Effects of Ncl overexpression in H9C2 cells (n=3). (**B**) SUnSET assay was used to assess global translation rate in H9C2 cells (n=3). (**C**) EU incorporation assay was performed to detect nascent rRNA synthesis (n=3). (**D**) Polysome profiling analysis was performed to evaluate ribosome distribution (n=3). (**E**) SA-β-gal staining was used to detect cellular senescence (n=3). (**F**) Western blot was used to determine p21 protein levels (n=3). (Kruskal-Wallis test). $p < 0.05$ (*), $p < 0.01$ (**), $p < 0.001$ (***).

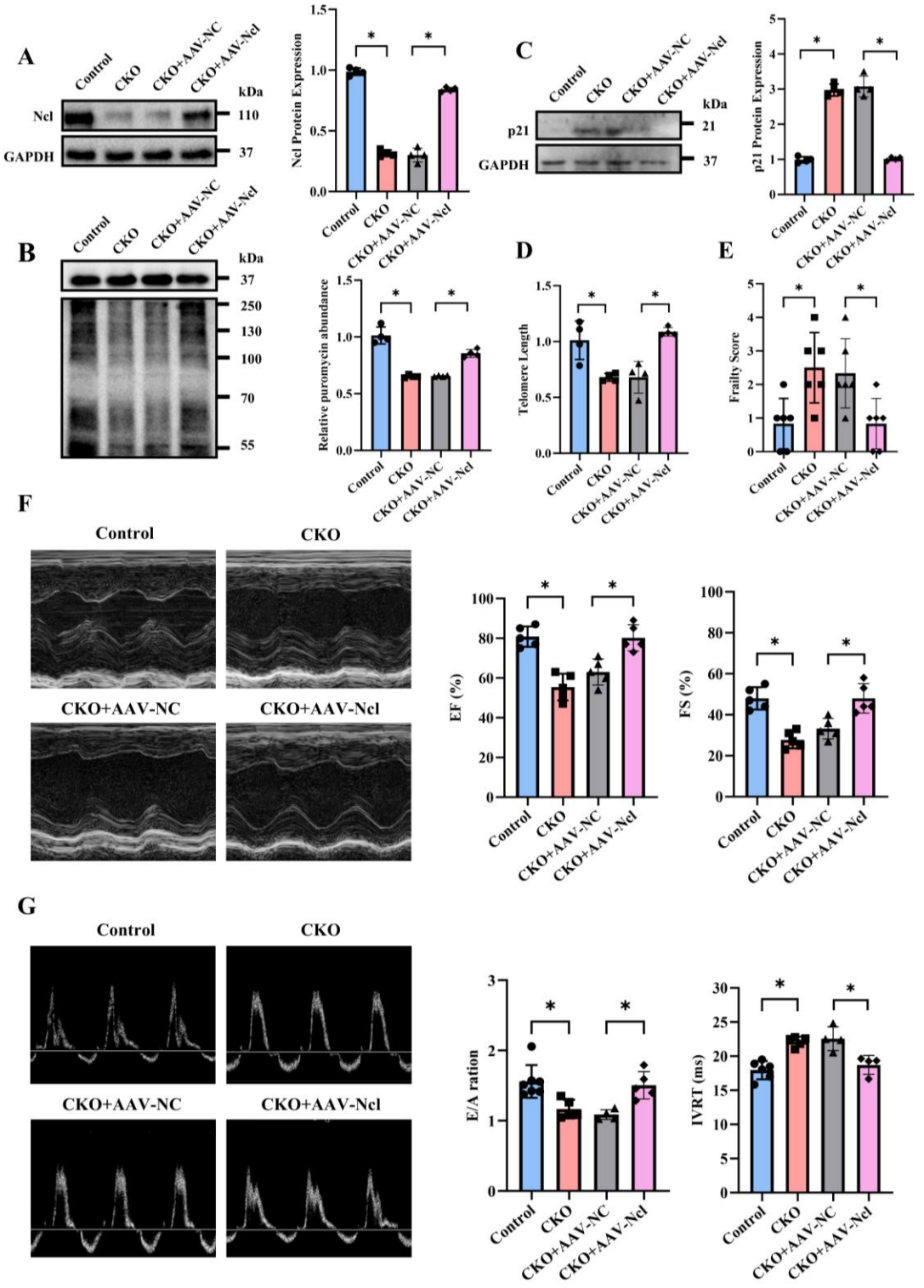

Figure 11. AAV9-mediated Ncl supplementation ameliorates cardiac aging phenotypes in CKO mice. (**A**) Western blot was used to determine Ncl protein levels in heart tissues (n=4). (**B**) SUnSET assay was used to assess global translation rate in heart tissues (n=4). (**C**) Western blot was used to determine p21 protein levels in heart tissues (n=4). (**D**) qRT-PCR was used to quantify relative telomere length in heart tissues (n=4). (**E**) Frailty score was assessed based on the Fried frailty phenotype (n=6). (**F**) Echocardiography was used to evaluate systolic function (n=5). (**G**) Echocardiography was used to evaluate diastolic function (n=4-7). (Kruskal-Wallis test). $p < 0.05$ (*), $p < 0.01$ (**), $p < 0.001$ (***).

AAV9-mediated Ncl overexpression rescues cardiac aging phenotypes in CKO mice

To determine whether Ncl is the primary downstream effector through which circHIPK3 regulates cardiac aging, we assessed whether the introduction of Ncl could rescue the detrimental effects of circHIPK3 deficiency on cardiac function. As described in our previously published study [33], to overexpress Ncl in the mouse heart, AAV9-Ncl (5×10^{12} genome copies/mouse) was administered via tail vein injection. AAV9 vectors were constructed and provided by Tsingke Biotechnology Co., Ltd. (Beijing, China) (Fig. 11A, S2I). Four weeks after AAV injection, cardiac function and molecular markers were assessed.

SUnSET assays revealed that the global translation rate, which was decreased in CKO mice, was significantly rescued by AAV9-Ncl treatment (Fig. 11B). We next examined markers of cellular senescence. Western blot analysis showed that p21 protein levels, which were elevated in CKO hearts, were substantially decreased upon Ncl overexpression (Fig. 11C). Furthermore, telomere length was significantly shortened in CKO mice but restored in the AAV9-Ncl group (Fig. 11D). Frailty assessment based on the Fried frailty phenotype revealed that CKO mice exhibited significantly higher frailty scores compared to control mice, indicating accelerated physiological decline. Notably, AAV9-Ncl treatment reduced the frailty score (Fig. 11E).

Echocardiographic analysis revealed that CKO mice injected with AAV9-NC exhibited significantly reduced EF and FS compared to control mice, and AAV9-Ncl administration in CKO mice restored both EF and FS (Fig. 11F). In addition, diastolic function was also recovered following Ncl reconstitution (Fig. 11G). Overall, these results demonstrate that AAV9-mediated Ncl overexpression is sufficient to rescue cardiac dysfunction, restore ribosome biogenesis and protein synthesis, and reverse senescence markers in CKO mice, confirming that Ncl acts as a critical downstream effector of circHIPK3 in cardiac aging.

DISCUSSION

In this study, we identified circHIPK3 as a key regulator of Ncl. circHIPK3 is highly expressed in the young heart and declines with age. We demonstrated that circHIPK3 directly binds to Ncl mRNA to enhance its stability, thereby preserving Ncl protein levels. The age-related decrease in circHIPK3 and the subsequent reduction in Ncl abundance resulted in severe impairment of ribosomal biogenesis. Concurrently, cellular aging induces a pathological shift in Ncl, causing its dynamic LLPS state to transform into a less fluid, "aged condensate" that critically compromises pre-rRNA processing and ribosome production. This cascade ultimately drives cardiomyocyte senescence and promotes the progression of cardiac aging phenotypes, such as functional deterioration and pathological remodeling. Therefore, restoring the circHIPK3-Ncl axis represents a promising strategy to counteract nucleolar dysfunction and delay cardiac aging (Fig. 12).

In recent years, disrupted ribosome homeostasis has been recognized as a central hallmark of cellular and organismal aging [34]. Our study situates this concept specifically within cardiac aging. We found that aged hearts exhibit not only a significant decline in ribosome biogenesis capacity but also a concurrent reduction in ribosomal protein expression. The nucleolar core protein Ncl was identified as a critical mediator linking circHIPK3 to this process. This finding aligns with work by Wei et al., whose multi-omics analysis confirmed that impaired ribosome biogenesis likely contributes to myocardial dysfunction by compromising protein synthesis, ultimately leading to abnormal cardiac structure and function in conditions such as hypertrophy, myocardial infarction, and congenital heart defects [35]. As a core protein involved in multiple stages—from rDNA transcription and pre-rRNA processing to ribosomal subunit assembly—Ncl was shown for the first time in this study to be downregulated during cardiac aging and positively regulated by circHIPK3. This insight provides a mechanistic explanation for the decline in protein synthesis capacity and the loss of proteostasis in the aged heart: the downregulation of circHIPK3 results in the depletion of Ncl, a key regulatory molecule, thereby triggering ribosome biogenesis failure.

Ribosome biogenesis is energetically expensive, and the aging heart is marked by mitochondrial dysfunction [36]. Emerging evidence suggests intricate crosstalk between the nucleolus and mitochondria, wherein mitochondrial stress signals can directly impact nucleolar function and ribosomal RNA synthesis [10]. The PERK-eIF2 pathway serves as a key sensor that couples energy availability to protein synthesis [37]. Given that circHIPK3 expression declines with age and its loss impairs ribosome biogenesis, it is plausible that circHIPK3 downregulation may be linked to altered energy signaling. Whether circHIPK3 downregulation is linked to altered energy signaling and whether it participates in this nucleolus–mitochondria communication remains an open question that warrants future investigation.

In this study, we innovatively link circRNA function to the physical biology of the nucleolus, specifically through LLPS. As a quintessential membraneless organelle, the nucleolus heavily depends on the dynamic physical microenvironment established by LLPS. Aging

disrupts this nucleolar phase separation equilibrium, and the accompanying disturbance in nuclear RNA homeostasis alters the availability of nuclear proteins, impairs polymerase initiation and binding, and reduces transcriptional efficiency. This disruption rapidly interferes with nucleolar transcription, ribosomal processing, and nuclear export, collectively leading to a shutdown of translation. These changes contribute to systemic functional decline, altered cellular states, and the promotion of senescence [38]. Our work provides new experimental support for this model by demonstrating that circHIPK3 silencing not only reduces Ncl expression but, more critically, alters the phase separation dynamics of Ncl protein itself. This finding echoes recent research showing that aberrant phase separation of the nuclear protein FUS prevents its proper chromatin association, disrupts the regulation of key genes and nucleolar function, and ultimately drives hematopoietic stem cell aging [39]. Furthermore, a recent study demonstrated that a lncRNA maintains the functional phase state of nucleolar prion-like proteins to facilitate rRNA processing, providing direct evidence that RNA molecules can serve as critical modulators of nucleolar LLPS and ribosome biogenesis [40]. These observations, together with our findings, suggest that both circular and linear non-coding RNAs may converge on the nucleolus to regulate phase separation dynamics and proteostasis during aging. Notably, we observe that cellular senescence directly reduces the LLPS fluidity of nucleolar proteins, leading to a loss of Ncl phase separation dynamics. This altered physical state likely impairs the efficiency and fidelity of Ncl in processes such as pre-rRNA processing, thereby serving as a direct trigger for ribosome biogenesis failure. Such phase separation abnormalities may initiate a vicious cycle: impaired ribosome biogenesis reduces the quality of protein synthesis, which subsequently diminishes the expression of key factors required to maintain normal phase separation, further exacerbating nucleolar dysfunction.

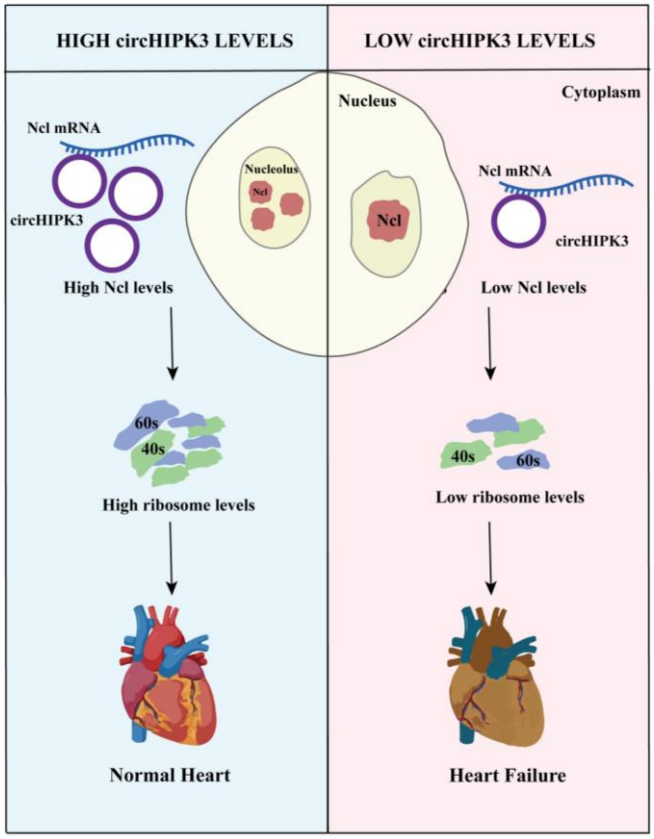

Figure 12. Schematic diagram of the regulatory mechanism. Under high circHIPK3 levels, circHIPK3 binds to Ncl mRNA to sustain its expression, thereby promoting ribosome biogenesis and maintaining normal cardiac function. In contrast, under low circHIPK3 levels, Ncl mRNA expression declines, ribosome biogenesis is reduced, and heart failure ensues. Meanwhile, during aging, alterations in Ncl LLPS occur, which further impairs ribosome biogenesis and exacerbates cardiomyocyte senescence.

At the upstream level of molecular mechanism, our study identifies a direct regulatory pathway independent of the classic ceRNA sponge model. Through systematic subcellular localization, CHIRP assays, and mRNA

stability tracking, we demonstrate that circHIPK3 interacts with the 5' UTR of Ncl mRNA and enhances its stability. This finding aligns with the evolving understanding of circRNA function, particularly the emerging paradigm in which circRNAs directly bind mRNAs to modulate their fate—a model recently elaborated in elsewhere [41]. In the absence of circHIPK3, the half-life of Ncl mRNA is markedly shortened, leading to reduced transcript levels and ultimately diminished protein synthesis. This discovery not only provides new evidence for circRNA-mediated post-transcriptional regulation but also suggests that direct circRNA-mRNA interactions may constitute an important layer of gene expression control. Notably, this mode of regulation likely offers high specificity, as the binding between circHIPK3 and Ncl mRNA relies on sequence-specific complementarity—a feature that could provide a theoretical foundation for developing precise therapeutic interventions.

The specificity of circHIPK3-mediated regulation stands in contrast to other circRNAs implicated in cardiac aging. For example, circFoxo3 has been shown to promote cardiac senescence through interactions with multiple stress-associated factors such as ID1 and E2F1, thereby modulating downstream signaling pathways [42]. In comparison, circHIPK3 operates at a more fundamental level by directly stabilizing Ncl mRNA and preserving its LLPS, thus safeguarding the core machinery of ribosome biogenesis. This mechanistic distinction positions circHIPK3 as a master regulator of nucleolar function and proteostasis during cardiac aging.

The findings of this study also possess significant translational potential. Given the central role of the circHIPK3-Ncl axis in cardiac aging, a range of intervention strategies can be explored. For example, delivering circHIPK3 mimics *via* nanocarriers could represent a novel therapeutic approach to delay cardiac aging [43]. Recent studies have demonstrated promising outcomes of circRNA-based therapies in models of ocular neurodegenerative diseases, providing strong support for our research direction [44]. Moreover, monitoring circHIPK3 levels in the blood could serve as a non-invasive biomarker for assessing individual cardiac aging. With the rapid advancement of liquid biopsy technology, the potential of circRNAs as diagnostic biomarkers for diseases is becoming increasingly prominent [45, 46].

Our study enhances the understanding of the molecular mechanisms underlying cardiac aging, especially by integrating non-coding RNA regulation, nucleolar phase-separation biophysics, and canonical ribosome metabolism pathways. It offers a novel theoretical foundation and potential intervention targets for preventing and mitigating cardiac aging and its related diseases. This multi-level research strategy reflects the latest direction in aging research. As emphasized in a recent review, deciphering the interplay across different biological levels during aging is crucial to unraveling the essence of aging [2]. Our work not only provides fresh insights into cardiac aging mechanisms, but also lays a theoretical groundwork for developing innovative therapeutic strategies against age-related heart failure, which aligns well with the current emphasis on precision medicine and targeted therapy in cardiology [47].

This study has several limitations to acknowledge. First, our findings are based on murine models and cardiomyocyte cell lines; validation in human cardiac tissues and clinical cohorts is needed to confirm the translational relevance of the circHIPK3-Ncl axis. Second, the role of circHIPK3 in non-cardiomyocyte cardiac cell types during aging remains uncharacterized. Additionally, while we observed altered Ncl LLPS dynamics upon circHIPK3 deficiency, the causal relationship requires direct validation. Future in vitro reconstitution experiments using purified components are needed to determine whether circHIPK3 directly modulates Ncl phase separation and ribosome biogenesis.

Conclusion

This study identifies the "circHIPK3-Ncl-ribosome biogenesis" axis as a critical regulator of cardiac aging. circHIPK3 exerts cardioprotective effects through dual regulation of Ncl: it stabilizes Ncl mRNA and supports Ncl LLPS, thereby ensuring proper ribosome biogenesis. The loss of circHIPK3 triggers cardiac senescence phenotypes, whereas its protective role suggests that circHIPK3 may serve as a potential diagnostic biomarker and warrants further investigation as a therapeutic candidate for age-related cardiovascular diseases.

Authors' contributions

HZ, TL designed the study, analyzed data, and wrote the manuscript. XL, YZ, AL, ZZ and HZ performed experiments and collected data. BL and YX interpreted the data and revised the manuscript. YL conceived and designed the study, analyzed data, and wrote the manuscript. All authors read and approved the final manuscript.

Availability of data and materials

The analyzed datasets generated during the present study are available from the corresponding author upon reasonable request..

Animal studies

All animal experiments were performed in accordance with the *NIH Guide for the Care and Use of Laboratory Animals* (NIH Publications No. 8023, revised 1978) and complied with the ARRIVE (Animal Research: Reporting of In Vivo Experiments) guidelines. The experimental protocol was reviewed and approved by the Animal Ethics Committee of the Institute of Cardiovascular Science, Soochow University.

Funding

This work was supported by the National Natural Science Foundation of China (82370264, 82570312, 81870194 and 91849122 to Y Li). National Expert Program of the Ministry of Human Resources and Social Security (7124600125 to Y Li). Hubei Key Laboratory of Embryonic Stem Cell Research, Hubei University of Medicine (No. 2025ESOF001 to Y Zhang). Project of State Key Laboratory of Radiation Medicine and Protection, Soochow University (No. GZK12023023 to Y Li). A Project Funded by the Priority Academic Program Development of Jiangsu Higher Education Institutions.

Declaration of competing interest

The authors state that they have no known competing financial or personal interests that could have seemed to influence the work reported in this study.

Supplementary Materials

The Supplementary data can be found online at: www.aginganddisease.org/EN/10.14336/AD.2026.0142

References

[1] Global Burden of Cardiovascular Diseases and Risks 2023 Collaborators (2025). Global, Regional, and National Burden of Cardiovascular Diseases and Risk Factors in 204 Countries and Territories, 1990-2023. J Am Coll Cardiol, 86(22):2167-2243.

[2] Wu Z, Qu J, Zhang W, Liu GH (2025). Biomarkers of ageing of humans and non-human primates. Nat Rev Mol Cell Biol, 26:826-847.

[3] Chen MS, Lee RT, Garbern JC (2022). Senescence mechanisms and targets in the heart. Cardiovasc Res, 118:1173-1187.

[4] Wang Q, Wang Y, Lin Y, Zhou J, Mao Z, Gu X, et al. (2025). Thymic Bmi-1 hampers γδT17 generation and its derived RORγt-IL-17A signaling to delay cardiac aging. Proc Natl Acad Sci U S A, 122:e2414717122.

[5] Sagmeister P, Rosch S, Fengler K, Kresoja KP, Gori T, Thiele H, et al. (2025). Running on empty: Factors underpinning impaired cardiac output reserve in heart failure with preserved ejection fraction. Exp Physiol, 110:694-707.

[6] Tang J, Yue L, Xu Y, Xu F, Cai X, Fu Y, et al. (2025). Longitudinal serum proteome mapping reveals biomarkers for healthy ageing and related cardiometabolic diseases. Nat Metab, 7:166-181.

[7] Lee S, Heinrich P, Lee D, Kang Y, Robinson H, Humphrey SJ, et al. (2025). IGFBP2 Mediates Human iPSC-Cardiomyocyte Proliferation in a Cellular Contact-Dependent Manner. Circ Res, 137:1279-1291.

[8] Thomson E, Ferreira-Cerca S, Hurt E (2013). Eukaryotic ribosome biogenesis at a glance. J Cell Sci, 126:4815-4821.

[9] Chen L, Wu B, Mo L, Chen H, Yin X, Zhao Y, et al. (2025). High-content screening identifies ganoderic acid A as a senotherapeutic to prevent cellular senescence and extend healthspan in preclinical models. Nat Commun, 16:2878.

[10] Snieckute G, Ryder L, Vind AC, Wu Z, Arendrup FS, Stoneley M, et al. (2023). ROS-induced ribosome impairment underlies ZAKα-mediated metabolic decline in obesity and aging. Science, 382:eadf3208.

[11] Di Fraia D, Marino A, Lee JH, Kelmer Sacramento E, Baumgart M, Bagnoli S, et al. (2025). Altered translation elongation contributes to key hallmarks of aging in the killifish brain. Science, 389:eadk3079.

[12] Shcherbakov D, Nigri M, Akbergenov R, Brilkova M, Mantovani M, Petit PI, et al. (2022). Premature aging in mice with error-prone protein synthesis. Sci Adv, 8:eabl9051.

[13] Shaw PJ, Jordan EG (1995). The nucleolus. Annu Rev Cell Dev Biol, 11:93-121.

[14] Tomkova K, Roman M, Adebayo AS, Sheikh S, Yusoff S, Gulston M, et al. (2024). Multimorbidity is associated with myocardial DNA damage, nucleolar stress, dysregulated energy metabolism, and senescence in cardiovascular disease. NPJ Aging, 10:58.

[15] Cangelosi D, Brignole C, Bensa V, Tamma R, Malaguti F, Carlini B, et al. (2022). Nucleolin expression has prognostic value in neuroblastoma patients. EBioMedicine, 85:104300.

[16] Srivastava M, Pollard HB (1999). Molecular dissection of nucleolin's role in growth and cell proliferation: new insights. Faseb j, 13:1911-1922.

[17] Deng H-f, Zou J, Wang N, Ma H, Zhu L-l, Liu K, et al. (2022). Nicorandil alleviates cardiac remodeling and dysfunction post -infarction by up-regulating the nucleolin/autophagy axis. Cellular Signalling, 92:110272.

[18] Sun H, Huang L, Liang P, Tang Y, Chen C, Chen H, et al. (2021). Nucleolin regulates the proliferation of vascular smooth muscle cells in atherosclerotic via Aurora B. J Cell Mol Med, 25:751-762.

[19] Chen L-L (2016). The biogenesis and emerging roles of circular RNAs. Nat Rev Mol Cell Biol, 17:205-211.

[20] Memczak S, Jens M, Elefsinioti A, Torti F, Krueger J, Rybak A, et al. (2013). Circular RNAs are a large class of animal RNAs with regulatory potency. Nature, 495:333-338.

[21] Enuka Y, Lauriola M, Feldman ME, Sas-Chen A, Ulitsky I, Yarden Y (2015). Circular RNAs are long-lived and display only minimal early alterations in response to a growth factor. Nucleic Acids Research, 44:1370-1383.

[22] Zheng Q, Bao C, Guo W, Li S, Chen J, Chen B, et al. (2016). Circular RNA profiling reveals an abundant circHIPK3 that regulates cell growth by sponging multiple miRNAs. Nat Commun, 7:11215.

[23] Ding F, Lu L, Wu C, Pan X, Liu B, Zhang Y, et al. (2022). circHIPK3 prevents cardiac senescence by acting as a scaffold to recruit ubiquitin ligase to degrade HuR. Theranostics, 12:7550-7566.

[24] Wu Y, Wei Y, Li Y, Dou Y, Yang Y, Liu H, et al. (2025). Sperm-Derived CircRNA-1572 Regulates Embryogenesis and Zygotic Genome Activation by Targeting CCNB2 via Bta-miR-2478-L-2. Adv Sci (Weinh), 12:e2414325.

[25] Yi J, Du J, Chen X, Nie RC, Hu GS, Wang L, et al. (2025). A circRNA-mRNA pairing mechanism regulates tumor growth and endocrine therapy resistance in ER-positive breast cancer. Proc Natl Acad Sci U S A, 122:e2420383122.

[26] Yan B, Zhang Y, Liang C, Liu B, Ding F, Wang Y, et al. (2020). Stem cell-derived exosomes prevent pyroptosis and repair ischemic muscle injury through a novel exosome/circHIPK3/FOXO3a pathway. Theranostics, 10:6728-6742.

[27] Ding JF, Liu ZY, Tu B, Gao L, Geng HR, Xu B, et al. (2026). RUNX1 N6-methyladenosine methylation enhances cytoskeleton remodeling and boosts cardiac fibrosis. Cardiovasc Res, 122:363-378.

[28] Banani SF, Lee HO, Hyman AA, Rosen MK (2017). Biomolecular condensates: organizers of cellular biochemistry. Nat Rev Mol Cell Biol, 18:285-298.

[29] Li Y, Liu Y, Yu XY, Xu Y, Pan X, Sun Y, et al. (2024). Membraneless organelles in health and disease: exploring the molecular basis, physiological roles and pathological implications. Signal Transduct Target Ther, 9:305.

[30] Jo M, Kim S, Park J, Chang YT, Gwon Y (2024). Reduced dynamicity and increased high-order protein assemblies in dense fibrillar component of the nucleolus under cellular senescence. Redox Biol, 75:103279.

[31] King MR, Ruff KM, Lin AZ, Pant A, Farag M, Lalmansingh JM, et al. (2024). Macromolecular condensation organizes nucleolar sub-phases to set up a pH gradient. Cell, 187:1889-1906.e1824.

[32] Park SK, Page GP, Kim K, Allison DB, Meydani M, Weindruch R, et al. (2008). alpha- and gamma-Tocopherol prevent age-related transcriptional alterations in the heart and brain of mice. J Nutr, 138:1010-1018.

[33] Geng S, Liu SB, He W, Pan X, Sun Y, Xue T, et al. (2024). Deletion of TECRL promotes skeletal muscle repair by up-regulating EGR2. Proc Natl Acad Sci U S A, 121:e2317495121.

[34] Gao F, Liang T, Lu YW, Fu X, Dong X, Pu L, et al. (2023). A defect in mitochondrial protein translation influences mitonuclear communication in the heart. Nat Commun, 14:1595.

[35] Wei S, Shen R, Lu X, Li X, He L, Zhang Y, et al. (2025). Mendelian randomization provides a multi-omics perspective on the regulation of genes involved in ribosome biogenesis in relation to cardiac structure and function. Clin Epigenetics, 17:42.

[36] Burtscher J, Soltany A, Visavadiya NP, Burtscher M, Millet GP, Khoramipour K, et al. (2023). Mitochondrial stress and mitokines in aging. Aging Cell, 22:e13770.

[37] Zhao Q, Sarinay Cenik E (2025). Is mitochondrial function at the heart of ribosome-related diseases? Trends Cell Biol, 35:815-818.

[38] Han X, Xing L, Hong Y, Zhang X, Hao B, Lu JY, et al. (2024). Nuclear RNA homeostasis promotes systems-level coordination of cell fate and senescence. Cell Stem Cell, 31:694-716.e611.

[39] Tang B, Wang X, He H, Chen R, Qiao G, Yang Y, et al. (2024). Aging-disturbed FUS phase transition impairs hematopoietic stem cells by altering chromatin structure. Blood, 143:124-138.

[40] Sun YM, Zhu SX, Chen XT, Pan Q, An Y, Chen TQ, et al. (2024). lncRNAs maintain the functional phase state of nucleolar prion-like protein to facilitate rRNA processing. Mol Cell, 84:4878-4895.e4810.

[41] Wu S, Xu H, Zhang R, Wang X, Yang J, Li X, et al. (2022). Circular RNA circLAMA3 inhibits the proliferation of bladder cancer by directly binding an mRNA. Mol Ther Oncolytics, 24:742-754.

[42] Du WW, Yang W, Chen Y, Wu ZK, Foster FS, Yang Z, et al. (2017). Foxo3 circular RNA promotes cardiac senescence by modulating multiple factors associated with stress and senescence responses. Eur Heart J, 38:1402-1412.

[43] Gil-Cabrerizo P, Simon-Yarza T, Garbayo E, Blanco-Prieto MJ (2024). Navigating the landscape of RNA delivery systems in cardiovascular disease therapeutics. Adv Drug Deliv Rev, 208:115302.

[44] Jiang W, Xiao D, Wu C, Yang J, Peng X, Chen L, et al. (2024). Circular RNA-based therapy provides sustained and robust neuroprotection for retinal ganglion cells. Mol Ther Nucleic Acids, 35:102258.

[45] Shi Y, Song R, Wang Z, Zhang H, Zhu J, Yue Y, et al. (2021). Potential clinical value of circular RNAs as peripheral biomarkers for the diagnosis and treatment of major depressive disorder. EBioMedicine, 66:103337.

[46] Li S, Wang J, Qiu L, Fu G, Li Y, Su Q, et al. (2024). Comprehensive circular RNA profiling provides insight into colorectal cancer pathogenesis and reveals diagnostically relevant biomarkers. Clin Transl Med, 14:e70049.

[47] Leopold JA, Loscalzo J (2018). Emerging Role of Precision Medicine in Cardiovascular Disease. Circ Res, 122:1302-1315.